Version 1.1, February 9, 2017
Preprint typeset using LaTeX style emulateapj v. 12/16/11

THE COSMIC SHORELINE: THE EVIDENCE THAT ESCAPE DETERMINES WHICH PLANETS HAVE ATMOSPHERES, AND WHAT THIS MAY MEAN FOR PROXIMA CENTAURI B

Kevin J. Zahnle[1]
NASA Ames Research Center, Moffett Field, CA 94035

and

David C. Catling[2]
Department of Earth and Space Sciences/Astrobiology Program, University of Washington, Seattle, WA

Version 1.1, February 9, 2017

ABSTRACT

The planets of the Solar System divide neatly between those with atmospheres and those without when arranged by insolation (I) and escape velocity ($v_{\rm esc}$). The dividing line goes as $I \propto v_{\rm esc}^4$. Exoplanets with reported masses and radii are shown to crowd against the extrapolation of the Solar System trend, making a metaphorical cosmic shoreline that unites all the planets. The $I \propto v_{\rm esc}^4$ relation may implicate thermal escape. We therefore address the general behavior of hydrodynamic thermal escape models ranging from Pluto to highly-irradiated Extrasolar Giant Planets (EGPs). Energy-limited escape is harder to test because copious XUV radiation is mostly a feature of young stars, and hence requires extrapolating to historic XUV fluences ($I_{\rm xuv}$) using proxies and power laws. An energy-limited shoreline should scale as $I_{\rm xuv} \propto v_{\rm esc}^3\sqrt{\rho}$, which differs distinctly from the apparent $I_{\rm xuv} \propto v_{\rm esc}^4$ relation. Energy-limited escape does provide good quantitative agreement to the highly irradiated EGPs. Diffusion-limited escape implies that no planet can lose more than 1% of its mass as H_2. Impact erosion, to the extent that impact velocities $v_{\rm imp}$ can be estimated for exoplanets, fits to a $v_{\rm imp} \approx 4 - 5\, v_{\rm esc}$ shoreline. The proportionality constant is consistent with what the collision of comet Shoemaker-Levy 9 showed us we should expect of modest impacts in deep atmospheres. With respect to the shoreline, Proxima Centauri b is on the metaphorical beach. Known hazards include its rapid energetic accretion, high impact velocities, its early life on the wrong side of the runaway greenhouse, and Proxima Centauri's XUV radiation. In its favor is a vast phase space of unknown unknowns.

Subject headings: planetary systems — stars: individual(Proxima Centauri)

1. INTRODUCTION

Volatile escape is the classic existential problem of planetary atmospheres (Hunten 1990). The problem has gained new currency with the discovery and characterization of exoplanets (Borucki et al. 2010; Lissauer et al. 2014). When escape is important it is likely to be rapid, and therefore relatively unlikely to be caught in the act, but the cumulative effects of escape should show up in the statistics of the new planets (Owen and Wu 2013; Lopez and Fortney 2014). In this paper we discuss the empirical division between planets with and without apparent atmospheres inside and outside of the Solar System. The paper is organized around four figures that compare the planets (dwarf and other) of the Solar System to the $\sim$ 590 exoplanets that were relatively well-characterized as of 26 August 2016. Then in Section 6 we address the place of Proxima Centauri b among these planets.

In Section 2 we compare total stellar radiation intercepted by a planet (insolation, I) to the planet's escape velocity ($v_{\rm esc}$). In previous work we found that on such a plot the empirical division between planets with and without atmospheres follows a $I \propto v_{\rm esc}^4$ power law that we have called the "cosmic shoreline" (Zahnle 1998a; Catling and Zahnle 2009; Zahnle and Catling 2013). We then compare the planets to the predictions of two different thermal escape models, one pertinent to small planets with condensed volatiles at the surface, and the other pertinent to giant planets that are close to their stars. We also compare the planets to the water vapor runaway greenhouse limit, which has a different relation to insolation and gravity.

In Section 3 we restrict stellar irradiation to extreme ultraviolet (EUV) and X-rays, here lumped together as XUV radiation ($I_{\rm xuv}$). The intent is to address the popular XUV-driven escape hypothesis (e.g., Hayashi et al. 1979; Sekiya et al. 1980a, 1981; Watson et al. 1981; Lammer et al. 2003a; Lecavelier et al. 2004; Yelle 2004; Tian et al. 2005; Erkaev et al. 2007; Garcia-Munoz 2007; Koskinen et al. 2009; Lammer et al. 2009; Murray-Clay et al. 2009; Tian 2009; Erkaev et al. 2013; Koskinen et al. 2013; Lammer et al. 2013; Owen and Wu 2013; Koskinen et al. 2014; Lammer et al. 2014; Lopez and Fortney 2014; Tian 2015; Erkaev et al. 2015, 2016; Owen and Alvarez 2016, the list is not complete). We estimate historic XUV fluences of the host stars to find that the shoreline also appears in XUV with the same power law, $I_{\rm xuv} \propto v_{\rm esc}^4$.

Section 4 begins by pointing out that the empirical $I_{\rm xuv} \propto v_{\rm esc}^4$ relation is not in accord with the basic predictions

[1] kevin.j.zahnle@NASA.gov
[2] dcatling@u.washington.edu

of energy-limited escape. We compare the predictions of the simplest quantitative energy-limited escape model to the apparent planets. Because XUV radiation is well-suited to driving the escape of hydrogen in particular, it is natural to discuss selective escape and diffusion-limited escape in the context of XUV-driven escape. We show here that diffusion-limited escape, where applicable, reduces to a general result that may be particularly germane to super-earths.

Section 5 addresses impact erosion. Impact erosion of planetary atmospheres offers a plausible alternative to thermal or irradiation-driven escape (Zahnle et al. 1992; Zahnle 1998a; Catling and Zahnle 2013; Schlichting et al. 2015). Here we compare impact velocities $v_{\rm imp}$ to escape velocities for the planets plotted in the previous figures. With impact erosion there is a reasonable expectation that a $v_{\rm imp} \propto v_{\rm esc}$ relationship should apply at all scales; the difficulty in testing the hypothesis is in estimating what the impact velocities should be.

Section 6 addresses Proxima Centauri b (which we will refer to as "Proxima b" for the rest of the paper because the star, which is uniquely the Sun's nearest neighbor, should really be just "Proxima"). In Section 6 we document how we plot Proxima b against the other planets and discuss its place with respect to the cosmic shoreline.

2. TOTAL INSOLATION VS. ESCAPE VELOCITY

Figure 1 plots relative insolation I against escape velocity $v_{\rm esc}$ for the adequately characterized planets. The figure shows that atmospheres are found where gravitational binding energy is high and total insolation is low. The figure also shows that the boundary between planets with and without apparent atmospheres is both well-defined and follows an empirical $I \propto v_{\rm esc}^4$ power law that extends from the planets of our solar system up through the known exoplanets.

For most solar system objects we use escape velocities from Zahnle et al. (2003). The Kuiper Belt Objects (KBOs) and Pluto/Charon have been updated to reflect more recent information (Rabinowitz et al. 2006; Brown and Schaller 2007; Brown 2013; Sicardy et al. 2011; Pál et al. 2012; Braga-Ribas et al. 2013; Fornasier et al. 2013; Lellouch et al. 2013; Wesley et al. 2013; Stern et al. 2015). The presence or absence of an atmosphere for solar system objects is indicated by filled or open symbols, respectively. For the solar system, what is meant by "having an atmosphere" is usually pretty obvious, but even here there are borderline cases, such as Io, which has a very thin volcanogenic SO_2 atmosphere. The KBOs are more ambiguous. A few of the largest retain stores of frozen methane on their surfaces. These are plotted in purple on Figure 1 as boxes-half-full. It is reasonable to suppose that their surface volatiles will evaporate when close to the Sun and they will then for a time have atmospheres similar to those of Pluto and Triton. This sort of seasonal transformation is very likely for Eris, which is currently near aphelion, and rather unlikely for Sedna, which is rather near its perihelion.

Figure 1 includes the nearly complete roster of transiting exoplanets with published radii and masses as of 26 August, 2016. For these planets, orbital parameters, diameters, and stellar luminosities are measured, albeit not always very precisely. A few planets are omitted because we were unable to estimate insolation. (Two exoplanets, KOI 55 b and KOI 55c, lie far above the bounds of Figure 1. These are interesting but peculiar worlds. The star KOI 55 is a hot blue subdwarf. It has already evolved through a red giant phase and is now becoming a white dwarf. The planets are very close to the star and very hot — of order 7000 K. They are smaller and denser than Earth, and presumably their atmospheres are made of silicates and metals.) The exoplanet.eu database (Schneider et al. 2011, http://exoplanet.eu) was filtered to include only exoplanets with (i) a reported radius R; (ii) a reported mass M; and (iii) a reported orbital period P. Radii and masses were used to compute escape velocities $v_{\rm esc}^2 = 2GM/R$. For most of the exoplanets the measured diameters and densities are typical of giant planets, which indicates that most of the transiting planets plotted on Figure 1 have atmospheres. Planets with radii $R_p > 8R_\oplus$ — Saturns and super-Saturns — are plotted as blue disks. Planets with radii $1.6R_\oplus < R_p < 8R_\oplus$ — Neptunes and sub-Saturns — are plotted as dark blue disks. Exoplanets with radii $R_p < 1.6R_\oplus$ — sub-Neptunes, Earths, and super-Earths — are plotted as green diamonds. This particular sorting by size appears to have some basis in fact (Lopez and Fortney 2014), with the three categories loosely corresponding to H_2-rich planets, H_2O-rich planets or H_2-enveloped rocky planets, and rocky planets.

For stellar luminosity we use the stellar radii $R_\star$ and stellar effective temperatures $T_\star$ listed for most of the central stars in the exoplanet.eu database.

$$L_{1\star} = 4\pi R_\star^2 \sigma T_\star^4. \tag{1}$$

If one or both of $R_\star$ and $T_\star$ is not listed, we estimate stellar luminosity using the visual magnitude m_v and stellar distance d (in parsecs) as reported in the exoplanet.eu database.

$$L_{2\star} = L_\odot \, (d/10)^2 \, 100^{0.2(4.83-m_v)}. \tag{2}$$

Here $m_v = 4.83$ is the visual magnitude of the Sun at 10 pc. For a few of the planets neither $L_{1\star}$ nor $L_{2\star}$ can be computed; these planets we omit. Insolation I is plotted as a dimensionless ratio relative to what is incident on Earth today. Insolation is computed using the planet's reported semimajor axis a if available, otherwise we estimate a from the stellar mass $M_\star$ and the period P

$$a^3 = \frac{GM_\star P^2}{4\pi^2} \tag{3}$$

in order to compute

$$I = \frac{L_\star}{L_\odot} \frac{a_\oplus^2}{a^2} \tag{4}$$

where $a_\oplus$ is the semimajor axis of Earth's orbit.

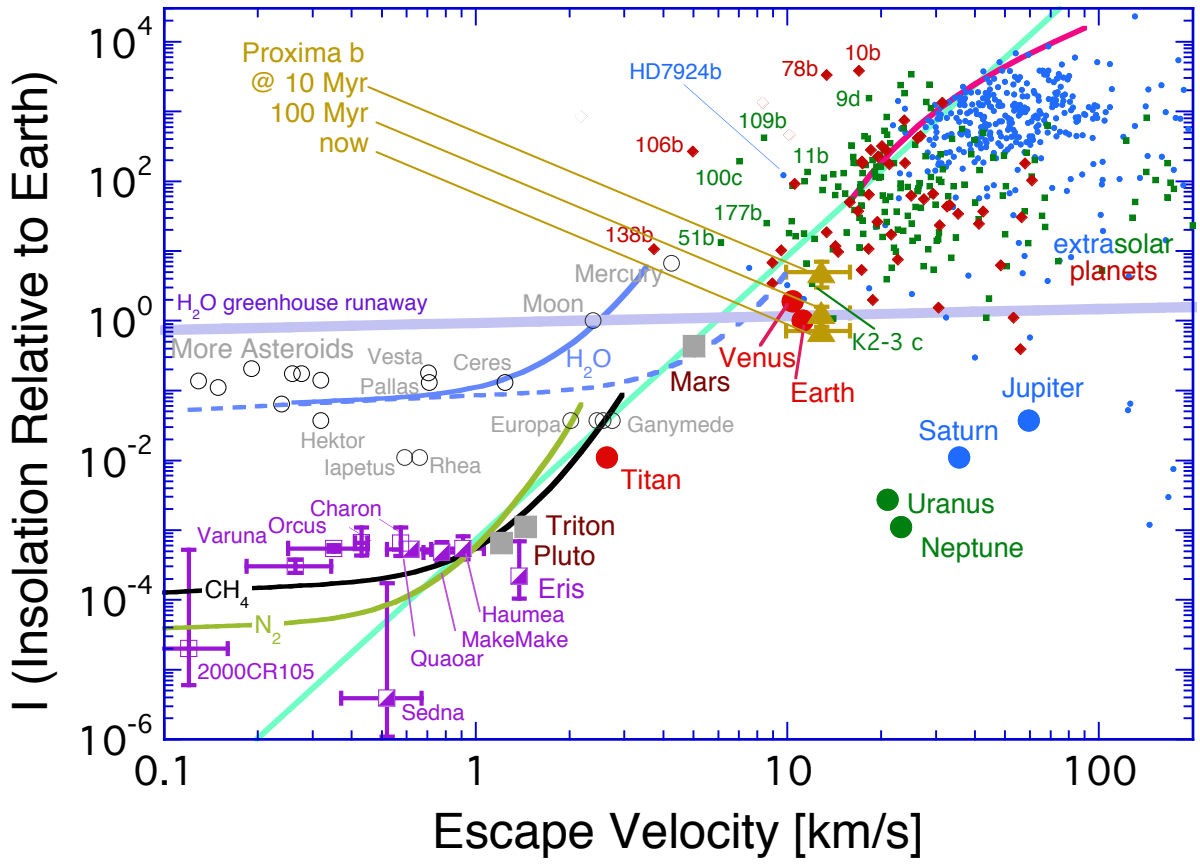

FIG. 1.— Atmospheres are found where gravity — here represented by the escape velocity — is high and insolation — here represented by the total stellar insolation at the planet relative to that received by Earth — is low. The presence or absence of an atmosphere on solar system objects is indicated by filled or open symbols, respectively. Extrasolar planets with known masses and radii as of 26 August, 2016 (Schneider et al. 2011, http://exoplanet.eu) are also plotted. The extrasolar planets are presented as blue disks if Saturn-like ($R > 8R_\oplus$), as green boxes if Neptune-like ($8R_\oplus > R > 1.6R_\oplus$), and as red diamonds if Venus-like ($R < 1.6R_\oplus$). The simple $I \propto v_{\rm esc}^4$ power law limning the cosmic shoreline is drawn by eye. Several of the more outlandish worlds are labeled by name; the abbreviation "10d" refers to "Kepler 10d." Error bars on the extrasolar planets are omitted for clarity, but many of the planets that plot to the left of the $I \propto v_{\rm esc}^4$ power law have very uncertain $v_{\rm esc}$; they may also be airless. Several models are also shown for comparison. Hydrodynamic thermal escape models for CH_4, N_2, and H_2O assume vapor pressure equilibrium at the surface. The two H_2O curves are for escape as H_2O (solid) or as H_2 (dashed). The magenta line is the thermal stability limit for hot Saturns as described in Section 2.4. The curvature is a consequence of tidal stripping. The magenta line bounds the giant Saturns as well as could be hoped, but as expected it does not bind the Neptunes. Also shown is the runaway greenhouse threshold for steam atmospheres. The models are described more fully in the text. Proxima b is plotted in gold at three times (10 Myr, 100 Myr, now) in the luminosity evolution of Proxima. It is very likely that Proxima b was born in a runaway greenhouse state and suffered extensive hydrogen losses as a super-Venus when young.

The general pattern seen in Figure 1 is what one would expect to see if escape were the most important process governing the volatile inventories of planets. Where the gravitational well is deep (measured by escape velocity), or where the influence of the central star is weak (measured here by insolation), planetary atmospheres are thick. Where the gravity is weak or the star too bright, there are only airless planets. It is curious that the non-giant planets in our Solar System that have atmospheres seem to be strung out along a single $I \propto v_{\rm esc}^4$ line, rather than scattered over the half-space below and to the right of the bounding line. A second surprise is that the known transiting extrasolar giant planets (EGPs) crowd against the extrapolation of that line. The $I \propto v_{\rm esc}^4$ line spans two orders of magnitude in escape velocity and nearly eight orders of magnitude in insolation. It is remarkable that a single power law should appear to relate hot EGPs at one extreme to Pluto and Triton at the other.

What Figure 1 does not show is what one might expect to see if the presence of atmospheres depended mostly on local nebular temperature (during accretion) or volatile supply. To put this another way, small warm worlds with significant atmospheres are missing. Such worlds are permitted if not mandatory in supply-side scenarios; indeed, active comets provide extreme examples of what such worlds can look like during their brief lives.

2.1. *Thermal escape from icy planets*

We consider isothermal atmospheres in which the major gas is in vapor pressure equilibrium with condensed volatiles at the surface. Our model resembles an earlier Jeans escape model used by Schaller and Brown (2007) to address thermal escape from Kuiper Belt objects, the chief difference is that we are addressing much faster escape rates in the hydrodynamic limit. We call these Clausius-Clapeyron (CC) atmospheres because they are controlled by vapor pressure (Lehmer et al. 2017). Clausius-Clapeyron atmospheres are fairly common in the solar system, with Pluto, Triton, and Mars being notable examples. Perez-Becker and Chiang (2013) investigated similar models for evaporation of very hot silicate planets. Although it is straightforward albeit messier to address polytropic atmospheres, or atmospheres that are saturated at all heights (Lehmer et al. 2017), or even saturated below a stratosphere, we have no evidence that real atmospheres would be better described by one of these models. A next-generation model needs to be able to accurately compute both the temperature and the mean molecular weight of the upper atmosphere. This is difficult. To illustrate: before the arrival of *New Horizons* at Pluto, several sophisticated models had predicted temperatures 40% higher than the true temperature and therefore escape rates orders of magnitude higher than the true escape rates (Gladstone et al. 2016). We are therefore content to construct isothermal models.

Isothermal hydrodynamic escape is described in terms of the isothermal sound speed $c_\circ^2 = k_B T_c/\bar{m}$, where T_c is the temperature and $\bar{m}$ is the mean molecular mass of the atmosphere. Pressure p is that of a perfect gas $p = \rho\, c_\circ^2$ with density ρ. The outflow is described in spherical (radial) geometry in steady state by continuity

$$\frac{\partial}{\partial r}\left(\rho u r^2\right) = 0, \tag{5}$$

where u is the outflow velocity and r is the radial coordinate increasing outward, and by the force balance of inertia, pressure, and gravity,

$$u\frac{\partial u}{\partial r} + \frac{1}{\rho}\frac{\partial p}{\partial r} = -\frac{GM}{r^2}, \tag{6}$$

in which M is the mass of the planet and G is the universal gravitational constant. These can be combined into a single isothermal planetary wind equation,

$$\left(u^2 - c_\circ^2\right)\frac{1}{u}\frac{\partial u}{\partial r} = \frac{2c_\circ^2}{r} - \frac{GM}{r^2}. \tag{7}$$

In a strongly bound atmosphere, $u^2 \ll c_\circ^2$ and $2c_\circ^2 \ll GM/r^2$ near the surface, so that $\partial u/\partial r > 0$. At large radii the geometric term $2c_\circ^2/r$ term eventually surpasses the gravity term and the right hand side of Eq 7 changes sign. At the critical distance r_c where $2c_\circ^2/r = GM/r^2$, zeroing the left hand side of Eq 7 requires either that $u^2 = c_\circ^2$ or that $\partial u/\partial r = 0$. The unique solution with $\partial u/\partial r > 0$, in which the velocity is equal to the sound speed $u_c = c_\circ$ at the critical point $r_c = GM/2c_\circ^2$, is the critical transonic solution for the wind and is the physical solution provided that the ram pressure of the wind ρu_c^2 at the critical point exceeds any background pressure exerted by interplanetary space.

Equation 7 is easily integrated for the upward velocity at the surface, u_s, in terms of the isothermal temperature T_c and the critical point conditions. Where escape is modest and $u_s^2 \ll c_\circ^2$,

$$u_s \approx c_\circ \left(\frac{r_c}{r_s}\right)^2 \exp\left(\frac{3}{2} - \frac{GM}{c_\circ^2 r_s}\right) \tag{8}$$

gives a good approximation to u_s. The density and pressure at the surface of a CC atmosphere are determined by the saturation vapor pressure at the surface temperature T_s,

$$\rho_s = \frac{\bar{m}\, p_s(T_s)}{k_B T_s}. \tag{9}$$

For display in Figure 1 we use empirical expressions for the vapor pressures of CH_4, N_2, and H_2O given by Fray and Schmidt (2009). For the isothermal CC atmosphere the rate of mass loss is a function of T_s and u_s

$$\dot{M} = 4\pi\rho_s u_s r_s^2. \tag{10}$$

The other determining equation is the balance between the power absorbed from sunlight and the sum of power radiated in the thermal infrared and power spent evaporating, heating, and lifting warm gas to space,

$$\frac{\pi R^2 L_\star}{4\pi a^2} = \frac{4\pi R^2 \sigma T_s^4}{1-\alpha} + \frac{GM\dot{M}}{R} + \dot{M}L_v, \tag{11}$$

where α is the Bond albedo, which for icy worlds we will take as $\alpha = 0.4$. The rightmost term takes into account the latent heat of vaporization L_v, an important part of the energy budget for small icy bodies. Here we are interested in whether a planet can hold an atmosphere for billions of years. In these cases escape is slow enough that the terms in Eq 11 involving $\dot{M}$ are negligible, so that the surface temperature is just the effective temperature.

Empirically, upper atmospheres of the CH_4-rich planets in the solar system are roughly twice as hot at high altitudes as they are at the surface (Table 1). The upper atmospheres are warm because (i) CH_4 absorbs sunlight and (ii)

TABLE 1
Surface temperatures and mesosphere temperatures of CH_4-rich atmospheres

Planet	Surface T_s	Mesosphere T_c	T_c/T_s	Reference
Titan	94	150-180	0.52 - 0.63	Koskinen et al. (2011)
Triton	38	50-60	0.63 - 0.76	Olkin et al. (1997)
Pluto	42	72	0.6	Gladstone et al. (2016)
Uranus	60*	110-150	0.4 - 0.55	Marten et al. (2005)
Neptune	60*	110-150	0.4 - 0.55	Marten et al. (2005)

* These are the effective temperatures.

CH_4 photolysis produces organic molecules and hazes that absorb sunlight, but at low temperatures neither CH_4 nor the hazes radiate as effectively as they absorb. The upper atmosphere temperatures are higher on Uranus and Neptune because the background gas is H_2, so that additional radiative coolants are limited to hydrocarbons like C_2H_2. On Titan, Triton, and Pluto, the background gas is N_2, which enables production of a wider variety of more efficient radiative coolants, HCN especially. For the CH_4-N_2 atmospheres of icy worlds we let reality be a guide and approximate the atmospheric temperature with $T_s = 0.6\,T_c$.

The black and green curves labeled "CH_4" and "N_2" are evaporation lines for the small icy planets. The density is set to $\rho = 2$ g/cm^3, similar to the densities of Triton, Titan, Ganymede, Callisto, and Pluto. The curves are computed for a star of age $\tau_\star = 5$ billion years and an atmophile mass fraction $\Delta M/M = 0.01$, where $\Delta M = \dot{M}\tau_\star$. It is interesting that the nominal curves "CH_4" and "N_2" resemble what is actually seen in the solar system. However, the results shown here are quite sensitive to $T_c/\bar{m}$ (the sound speed, squared), and consequently they are insensitive to everything else. We can regard the CC model as a descriptive model, in the sense that it provides a plausible explanation of what is observed, but it may prove difficult to implement as a prescriptive model, because in general T_c and $\bar{m}$ are hard to predict theoretically.

The solid blue curve is the comparable $\tau_\star = 5$ Gyr evaporation line for H_2O from planets scaled from volatile-enriched versions of Earth ($\rho = 5.5$, $\Delta M/M = 0.01$), Europa ($\rho = 3$ g/cm^3, $\Delta M/M = 0.1$), and Ganymede ($\rho = 2$, $\Delta M/M = 0.5$) — by chance these three cases are nearly indistinguishable on this plot, so we show them as one curve. For these models we set $T_c = T_s$ as, unlike the case for N_2-CH_4 atmospheres, we know of no good reason nor have we seen much evidence to suggest that the upper atmospheres of watery worlds should be especially hot or cold. Recall that here we are addressing thermal escape driven by the total irradiation from the central star; we will address escape from hot thermospheres heated by XUV radiation in Section 4 below.

The blue water line is to the asteroids as the methane line is to the KBOs, whether by accident or design, but unlike the case for the methane line, which approaches Pluto, Triton, and Titan, the water line comes nowhere close to explaining the terrestrial planets. The water line can be moved into the vicinity of the terrestrial planets by raising $c_\circ^2 = k_B T/\bar{m}$ by an order of magnitude. This can be done either by converting the H_2O to H_2 or by invoking a hot upper atmosphere. The result of raising $c_\circ^2$ is illustrated by the dashed blue curve, computed from the same CC model as for water but with $\bar{m} = 2m_{\rm H}$. Such a model may also be relevant to Hayashi-like primary nebular atmospheres, as it is reasonable to anticipate chemical equilibration and exchange between H_2, H_2O, and silicates at the surface if the atmosphere is deep (Hayashi et al. 1979; Sekiya et al. 1980a, 1981; Ikoma and Genda 2006).

2.2. *The water vapor runaway greenhouse*

The runaway greenhouse threshold is expected to be a weak function of planetary parameters. To illustrate, assume that the runaway greenhouse limit is set by a troposphere saturated with water vapor becoming optically thick (Nakajima et al. 1992). In the absence of pressure broadening, optical depth τ will scale as the column depth; with pressure broadening this will be multiplied by the pressure to a power ξ on the order of unity (Robinson and Catling 2012, 2014). For a pure water vapor atmosphere, these considerations imply that (Goldblatt 2015)

$$\tau = \kappa \frac{p_{\rm vap}^{1+\xi}}{g}, \tag{12}$$

where κ is an opacity. If we approximate the vapor pressure of water by a simple exponential

$$p_{\rm vap} = p_w \exp\left(-T_w/T\right), \tag{13}$$

with $T_w = 6000$ K and $p_w = 2.1 \times 10^7$ bars, the runaway greenhouse limit should scale as

$$I_r \propto T^4 \propto \left(\frac{(1+\xi)\,T_w}{\ln\left(\kappa p_w^{1+\xi}/g\right)} \right)^4, \tag{14}$$

an expression that is well approximated over the range of interest by $I_r \propto g^{0.2/(1+\xi)}$. The surface gravity g is expressed in terms of $v_{\rm esc}$ and planet density ρ by $g^2 \propto \rho v_{\rm esc}^2$. This leaves

$$I_r \propto \left(v_{\rm esc}^2\,\rho\right)^{0.1/(1+\xi)}. \tag{15}$$

This relation is plotted with $\xi = 1$ and $\rho = 3$ on Figure 1 as the "H_2O runaway greenhouse." It is scaled to Earth with the runaway set at 1.2 solar constants (Goldblatt et al. 2013; Yang et al. 2013; Wolf and Toon 2015; Leconte et al. 2013a).

2.3. *The Moon*

Figure 1 shows the Moon rising above the intersection of the water lines. In all likelihood the apparent desiccation of the Moon is a memory of how the Moon was made rather than the ruin of a more promising world, but as plotted here, the Moon as a habitable world appears to be marginally unstable against both thermal escape and the runaway greenhouse. Today, most of the lunar surface is unstable to Jeans escape of water (e.g., Catling and Kasting 2017, p. 138). When viewing the Moon from the viewpoint of terraforming it, both problems would be made more tractable by providing abundant heavy ballast gases to reduce the atmosphere's scale height.

2.4. *Extrasolar Giant Planets*

Here we address thermal evaporation of Extrasolar Giant Planets (EGPs). The topic has been addressed elsewhere (e.g., Owen and Wu 2013) with much more sophisticated models than we employ here, but for our purposes it seems best to hold to the isothermal approximation, which has the advantage of being analytic and easy to work with. Models of silicate-rich gas giants have tended to predict warm or even hot upper atmospheres, because small molecules made of rock-forming elements such as TiO are better absorbers of visible light than they are emitters of thermal infrared radiation. For the most part observations seem unsupportive. A difference from the icy worlds is that these planets are close enough to their stars that tidal truncation must be taken into account. This is conveniently done in terms of the Hill sphere distance defined by

$$r_h = a\left(\frac{M}{3M_\star}\right)^{1/3} \tag{16}$$

where as above a refers to the star-planet distance and $M_\star$ to the mass of the star (Erkaev et al. 2007). Along the star-planet axis Eq 6 becomes

$$u\frac{\partial u}{\partial r} + \frac{1}{\rho}\frac{\partial p}{\partial r} = -\frac{GM}{r^2} + \frac{GMr}{r_h^3}, \tag{17}$$

and Eq 7 becomes

$$\left(u^2 - c_\circ^2\right)\frac{1}{u}\frac{\partial u}{\partial r} = \frac{2c_\circ^2}{r} - \frac{GM}{r^2} + \frac{GMr}{r_h^3}. \tag{18}$$

Equation 18 assumes spherical symmetry for tidal forces, which is not a good assumption. Its crudeness is probably comparable to treating irradiation as globally uniform or the temperature as isothermal. The critical point is found by solving the cubic for r_c

$$\frac{2c_\circ^2}{r_c} - \frac{GM}{r_c^2} + \frac{GMr_c}{r_h^3} = 0. \tag{19}$$

Equation 18 is easily integrated analytically,

$$ur^2 = u_c r_c^2 \exp\left\{\frac{1}{2}\frac{u^2}{c_\circ^2} - \frac{1}{2}\frac{u_c^2}{c_\circ^2} + \frac{GM}{c_\circ^2 r_c} - \frac{GM}{c_\circ^2 r} + \frac{1}{2}\frac{GMr_c^2}{c_\circ^2 r_h^3} - \frac{1}{2}\frac{GMr^2}{c_\circ^2 r_h^3}\right\}. \tag{20}$$

Note that $u(r)$ is independent of density. Near the surface, where $u^2 \ll c_\circ^2$, Eq 20 can be rewritten as an equation for the flow velocity at the surface u_s using the critical point conditions. The flux at the surface $\rho_s u_s$ is obtained by multiplying by the surface density ρ_s.

$$\rho_s u_s = \rho_s c_\circ \frac{r_c^2}{r_s^2}\exp\left\{-\frac{1}{2} + \left(1 - \frac{r_s^2}{r_c^2}\right)\left(\frac{GM}{2r_c c_\circ^2} - 1\right) + \left(1 - \frac{r_s}{r_c}\right)\frac{GM}{r_c c_\circ^2}\right\} \tag{21}$$

To use Equation 21 requires choosing ρ_s at the lower boundary using other information.

In EUV- and XUV-driven escape studies, the lower boundary is typically set at the homopause or at the base of the thermosphere, with the latter defined by a monochromatic optical depth in XUV radiation (e.g., Watson et al. 1981; Tian et al. 2005; Lammer et al. 2013). The homopause can be a reasonable *a priori* choice if escape is sluggish enough that a homopause exists. However, as we show below in Section 4.2, for a gas giant to evaporate in 5 Gyrs, the flux of hydrogen to space is too great by orders of magnitude for a homopause to exist. In a full-featured hydrocode simulation of an XUV-heated wind, the lower boundary condition can be justified *a postiori* as self-consistent for a particular model by showing the model to be insensitive to changing it (e.g., Watson et al. 1981; Murray-Clay et al. 2009; Owen and Alvarez 2016).

In the simplest picture a gas giant does not have a well-defined surface. Under these conditions the whole planet takes part in the flow to space, with the source of the escaping gas being the shrinking or rarefaction of the interior. To first approximation, all EGPs have roughly the same radius; the typical radius of a hot Jupiter is 84,000 km (Fortney et al. 2007). Constant radius is a property of polytropes with a $p = K\rho^2$ equation of state. The radius is $R = \sqrt{2K/4\pi G}$, where G is the Newtonian gravitational constant (Hubbard 1973). Using observed radii of the known roster of transiting planets gives $K = 3 \pm 1 \times 10^{12}$ cm^5 g^{-1} s^{-2}. The interior is described by an analytic solution

$$\rho(r) = \frac{\pi M}{4R^3}\frac{R}{\pi r}\sin\left(\frac{\pi r}{R}\right). \tag{22}$$

We set the lower boundary where the inner polytrope and the outer isothermal envelope meet; i.e. where the polytropic pressure equals the pressure of an ideal gas at the planet's effective temperature $T_{\rm eff}$. This gives

$$\rho_{\rm lbc} = c_{\circ}^2/K \tag{23}$$

The other equation pertinent to escape is the global energy balance,

$$\frac{\pi R^2 L_\star}{4\pi a^2} = \frac{4\pi R^2 \sigma T_s^4}{1-\alpha} + \frac{GM\dot{M}}{R}\left(1 - \frac{3}{2}\frac{R}{r_h} + \frac{1}{2}\frac{R^3}{r_h^3}\right) + \dot{M}c_p\left(T_c - T_s\right) \tag{24}$$

The terms involving $\dot{M}$ are the work done against gravity and any excess heat left in the gas as it escapes. As was the case in Section 2.1 above, if thermal escape is extended over 5 billion years, the $\dot{M}$ terms in Eq 24 are negligible, and Eq 24 reduces to the usual expression for effective temperature,

$$\frac{L_\star}{4\pi a^2} \approx \frac{4\sigma T_{\rm eff}^4}{1-\alpha}. \tag{25}$$

For the EGPs we set the Bond albedo $\alpha = 0.1$, $\bar{m} = 2.4 m_{\rm H}$, $R_s = 8.4 \times 10^9$ cm, and in keeping with the isothermal assumption, we set $T_c = T_s = T_{\rm eff}$. The magenta curve in the upper-right-hand region of Figure 1 is computed for complete evaporation of the planet in $\tau_\star = 5$ Gyrs; i.e., we solve Eqs 21, 23, and 24 for $v_{\rm esc}$ such that $\dot{M}\tau_\star = M$. The simple model bounds the population of EGPs (blue disks) rather nicely. We stress that this is not an XUV-driven escape model. The planet evaporates because the planet is thermally unstable, not because XUV heating is removing the outer atmosphere.

3. XUV-DRIVEN ESCAPE

Stellar EUV and X-ray radiation can be very effective at driving the escape of H and H_2 from young planets (Hayashi et al. 1979; Sekiya et al. 1980a). Urey (1952) put it succinctly, "Hydrogen would absorb light from the sun in the far ultra-violet and since it does not radiate in the infra-red [it] would be lost very rapidly." Urey (1952) regarded hydrogen escape as obvious and an essential process in planetary evolution (and of habitable Earth in particular), but he did not quantify it. Hayashi et al. (1979) proposed that massive hydrogen-rich atmospheres of young planets were removed by copious EUV ("extreme ultraviolet," $\lambda < 100$ nm) and X-ray ($\lambda < 20$ nm) radiations from young stars (Sekiya et al. 1980a, 1981). Hayashi's idea has proved fruitful and subsequent work on EUV and X-ray driven escape has been voluminous (see Tian (2015) and Catling and Kasting (2017) for recent reviews). EUV and X-ray radiations are usually linked in the literature as XUV radiation because they are expected to be related in stars, and X-rays are more easily observed. We will use the XUV notation here.

In practice it is challenging to test the XUV hypothesis because the bulk of the XUV that a star emits in its lifetime is emitted when the star is very young, and hence for all but the youngest exoplanets the relevant stellar XUV fluxes are not observables. Rather, each star's ancient XUV flux needs to be reconstructed from imperfectly known empirical relationships that link stellar age and spectral type with observed XUV emissions. For our purposes, the matter is made fuzzier by the uncertainty that surrounds the fiducial star — our Sun — as different extrapolations differ markedly for the Sun when young.

Lammer et al. (2009) scaled XUV fluxes both with age and with spectral type for F, G, K, and M stars. They give two part power laws of the general form $L_{\rm xuv} \propto t_\star^{-\beta}$, with relatively shallow slopes ($\beta < 1$) before 0.6 Gyr and relatively steep slopes ($\beta > 1$) thereafter. In this prescription the cumulative XUV flux is a well-defined integral dominated by the saturated phase. We performed these integrals and generalized their result to a simple power law

$$L_{\rm xuv} \propto L_\star^{0.4} \tag{26}$$

which we then express in normalized form for plotting on Figure 2 as

$$I_{\rm xuv} = \frac{a_\oplus^2}{a^2}\left(\frac{L_\star}{L_\odot}\right)^{0.4} = I\left(\frac{L_\star}{L_\odot}\right)^{-0.6}. \tag{27}$$

The scaling in Figure 2 is therefore with respect to a model of the total cumulative XUV radiations emitted by the ancient Sun, including the early saturated phase.

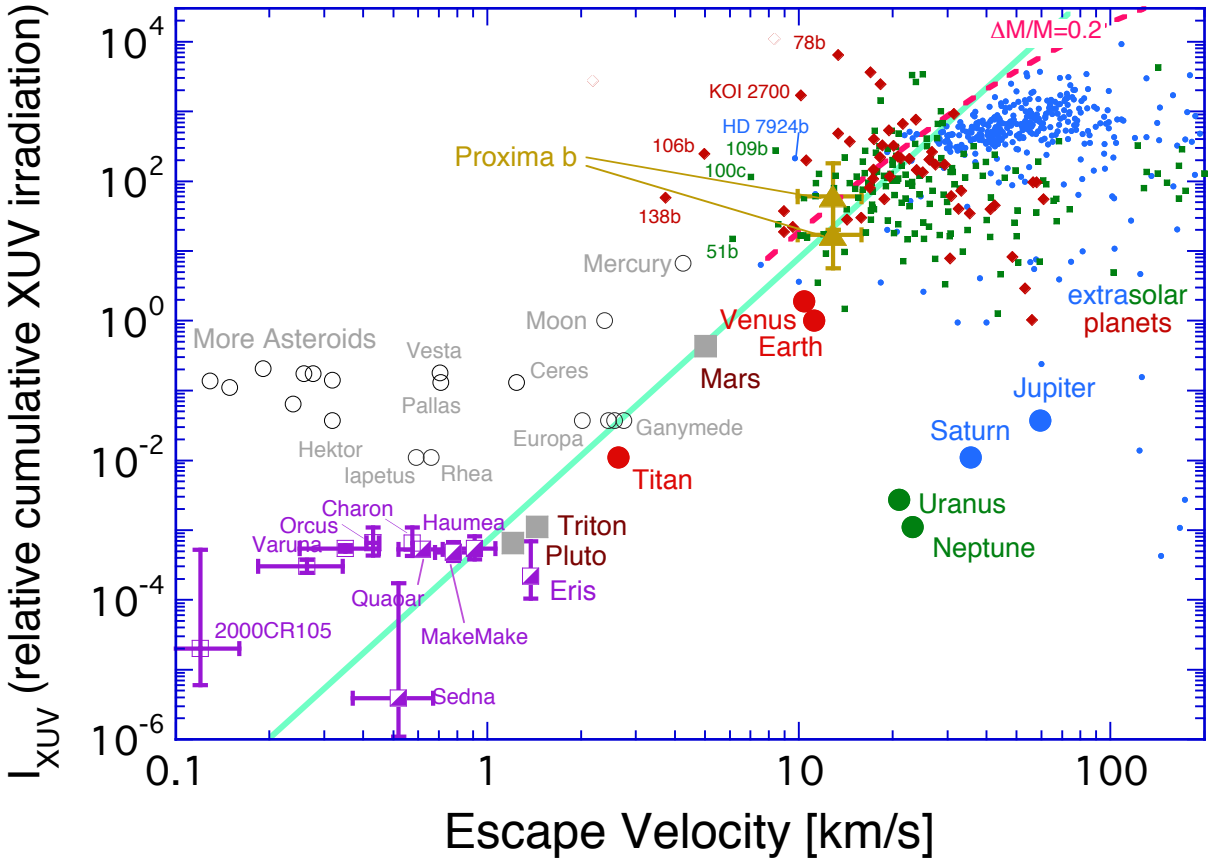

FIG. 2.— The analog to Figure 1 for estimated cumulative XUV irradiation, which is often hypothesized to be the driving force behind planetary evaporation (Tian 2015). Uncertainties are much larger here than in Figure 1 because all the XUV fluences need to be reconstructed, including the normalizing XUV fluence for Earth. No attempt is made to estimate errors for planets outside the solar system. The $I_{\rm xuv} \propto v_{\rm esc}^4$ line is drawn by eye. The dashed magenta curve is for XUV-driven energy-limited escape from tidally-truncated hot EGPs. It is labeled by fractional mass lost $\Delta M/M$. The model is described in Section 4.3 below.

Not surprisingly, Figure 2 looks a lot like Figure 1, since only the exoplanets have been changed. It is interesting that the EGPs (blue disks) in particular form a tighter distribution, which may be a hint that with XUV we are on the right track. The $I_{\rm xuv} \propto v_{\rm esc}^4$ line is drawn in by hand to guide the eye. The dashed magenta curve represents the quantitative predictions of a basic XUV-driven escape model to be described below in Section 4.3. That the XUV-driven escape model works rather well for EGPs is worth noting.

4. XUV-DRIVEN ESCAPE: PART II

In this section we address the expected form an energy-limited power law would take, and compare these predictions to those of XUV driven escape (Figure 3).

4.1. *General considerations*

It is possible to quantify the predictions of the XUV hypothesis if the escape is energy limited. Energy-limited escape is expected if the XUV radiation is too great for the incident radiation can be thermally conducted to the lower atmosphere (Watson et al. 1981)). If tidal truncation is for the moment neglected, the energy-limited escape can be expressed as

$$\dot{M}_{\rm el} = \frac{\eta \pi R^3 L_{\rm xuv}(t)}{4\pi a^2 G M} \tag{28}$$

where η is an efficiency factor that is usually taken to be $0.1 < \eta < 0.6$ (e.g., Lammer et al. 2013; Owen and Wu 2013; Koskinen et al. 2014; Bolmont et al. 2017). The mass loss efficiency η is less than the heating efficiency (fraction of incident XUV energy converted to heat) because the escaping gas is hotter, more dissociated, and more ionized than it was before it was irradiated. The factor η is a function of T, being smaller in cooler gas (< 3000 K) in which H_3^+ is a major radiative coolant (Koskinen et al. 2014) and smaller in hot gas ($\sim 10^4$ K) in which collisionally excited Lyman

α is a major coolant (Murray-Clay et al. 2009). In a steam atmosphere, FUV ("far ultraviolet," $100 < \lambda < 200$ nm) can also be important because it is absorbed by H_2O, O_2, and CO_2, provided irradiation is modest enough to leave the molecules intact (Sekiya et al. 1981). The contribution of FUV is implicitly folded into η. The total mass loss

$$\Delta M_{\rm el} = \int_0^{\tau_\star} \dot{M}_{\rm el}\, dt \tag{29}$$

is obtained by integrating the star's XUV radiation history expressed in terms of the Sun's history using $I_{\rm xuv} = (L_{\rm xuv}/L_{\rm xuv\odot})\,(a_\oplus/a)^2$. For the XUV history of the Sun itself we follow Ribas et al. (2005, 2016).

$$\begin{aligned} L_{\rm xuv\odot} &= L_x\,(t/t_x)^{-\beta} \qquad t > t_x \\ L_{\rm xuv\odot} &= L_x \qquad\qquad\qquad\quad t < t_x \end{aligned} \tag{30}$$

where $t_x = 0.1$ Gyr, $\beta = 1.24$, and where

$$L_x = 1.6 \times 10^{30}\,(t_x/t_\odot)^{-\beta} \quad \text{ergs s}^{-1} \tag{31}$$

is the saturated upper bound on the Sun's youthful excess. Cumulative escape is then

$$\frac{\Delta M_{\rm el}}{M} = \frac{\eta L_x t_x}{a_\oplus^2}\sqrt{\frac{3G}{8\pi}}\frac{I_{\rm xuv}}{v_{\rm esc}^3\sqrt{\rho}}\frac{1}{\beta-1}\left(\beta - (t_x/\tau_\star)^{\beta-1}\right) \tag{32}$$

which can be rearranged as a linear relation between $I_{\rm xuv}$ and x

$$I_{\rm xuv} = x\sqrt{\frac{8\pi}{3G}}\frac{\Delta M_{\rm el}}{M}\frac{a_\oplus^2\,(\beta-1)}{\eta L_x t_x\left(\beta - (t_x/\tau_\star)^{\beta-1}\right)} \tag{33}$$

with x defined by

$$x \equiv v_{\rm esc}^3\sqrt{\rho}. \tag{34}$$

Results are plotted in terms of the parameter x on Figure 3 for $\eta = 0.2$ as green lines and labeled for a range of lost masses $2 \times 10^{-4} \le \Delta M_{\rm el}/M \le 0.2$. As in Figure 2, we apply $L_{\rm xuv} \propto L_\star^{0.4}$ to the data in order to present a single relation that spans all the planets. The Solar System is fit by $\Delta M_{\rm el}/M \approx 0.001$, a trend that does not extend to the exoplanets, which are better matched by $\Delta M_{\rm el}/M \approx 0.1$.

4.2. *Diffusion-limited escape*

The diffusion-limited flux gives the upper bound on how quickly hydrogen can selectively escape by diffusing through a heavier gas that does not escape; more properly, it is the upper limit on the difference between hydrogen escape and heavy-constituent escape. It is often thought of in the context of vigorous hydrogen escape driven by XUV radiation (Sekiya et al. 1980b; Zahnle and Kasting 1986; Hunten et al. 1987), but it is quite general (Hunten and Donahue 1976). The diffusion-limited flux regulates hydrogen escape or H_2 abundance on Venus, Earth, Mars, and Titan today (see review by Catling and Kasting 2017, Chapter 5). It is likely that, should the diffusion-limited flux be smaller than the energy limit, the H_2 mixing ratio $f(H_2)$ will increase until the two limits are equal, as seen on Titan and Mars. But if $f(H_2) \to 1$ and the energy limit still exceeds the diffusion limit, it is not obvious what happens. The atmosphere may either escape as a whole (although the heavier gases escape more slowly, so that the remnant atmosphere becomes mass fractionated), or hydrogen escape is throttled to the diffusion limit and the excess energy is radiated to space by the heavy gases. A possible example of escape at the diffusion limit among the EGPs is HD 209458b (Vidal-Madjar et al. 2003, 2004; Yelle 2004; Koskinen et al. 2013).

The upper bound on the escape flux of a gas species of molecular mass m_i from a static gas atmosphere of molecular mass m_j ($m_i < m_j$) in the diffusion limit from an isothermal atmosphere is

$$\phi_{i,\rm dl} = f_i\frac{GM\,(m_j - m_i)}{R^2}\frac{b_{ij}}{kT}, \tag{35}$$

where f_i is the mixing ratio of the light gas and b_{ij} is the binary diffusion coefficient between the two species i and j. Typically $b_{ij} \propto T^{0.75}$. The corresponding mass loss rate is

$$\dot{M} = 4\pi R^2 m_i \phi_{i,\rm dl}. \tag{36}$$

The timescale for losing an atmosphere of mass $\Delta M_{\rm dl}$ is $\tau_{\rm dl} = \Delta M_{\rm dl}/\dot{M}$. The upper bound that diffusion puts on atmospheric escape can be written

$$\frac{\Delta M_{\rm dl}}{M} = \frac{4\pi m_i f_i\,(m_j - m_i)\,b_{ij} G\tau_{\rm dl}}{kT}. \tag{37}$$

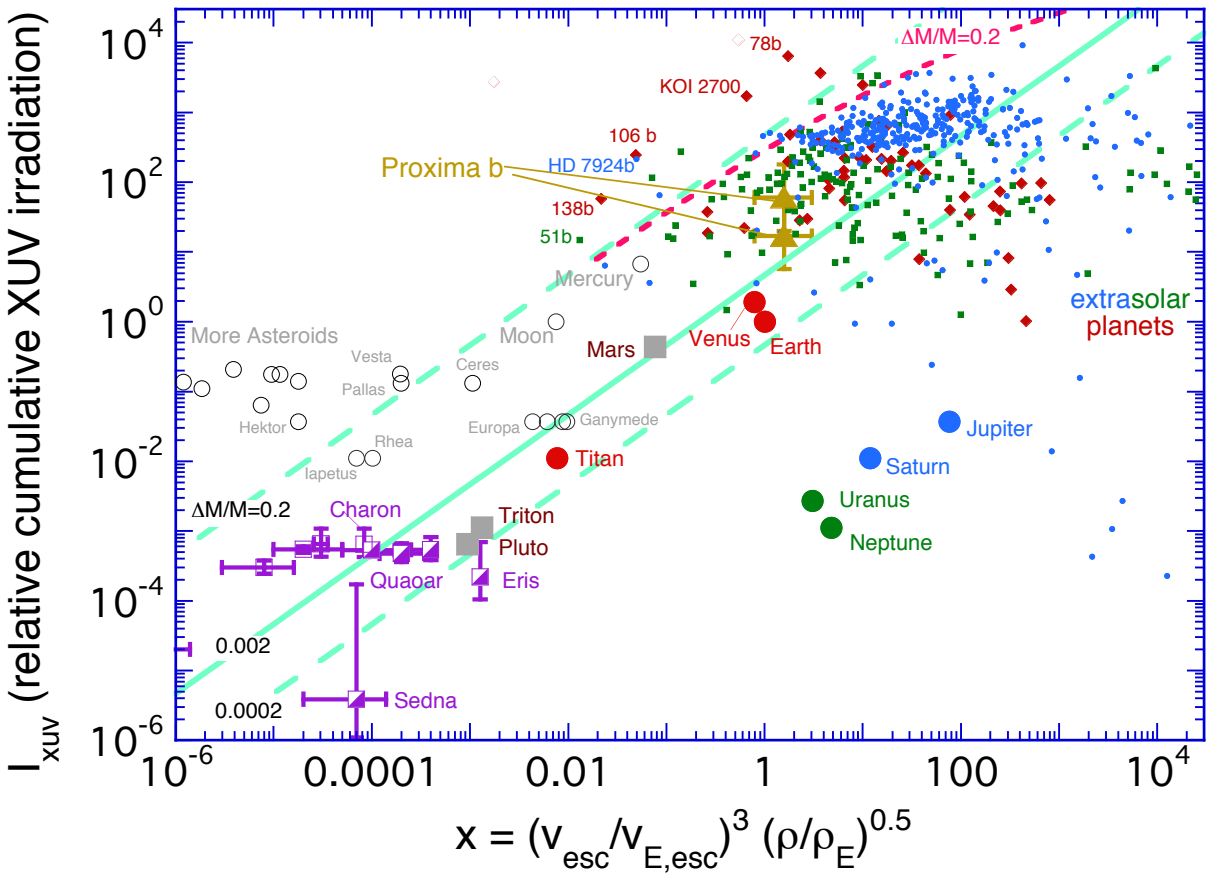

FIG. 3.— Here the data from Figure 2 are plotted against the expectations of the simplest theory. Energy-limited models predict that, if tidal stripping is unimportant, the insolation $I_{\rm xuv}$ should be linearly proportional to the quantity $x \equiv v_{\rm esc}^3 \sqrt{\rho}$. Here we express x as normalized to Earth, $(v_{\rm esc}/v_{\oplus{\rm esc}})^3 \sqrt{\rho/\rho_\oplus}$, so that Earth sits at $(1,1)$. The green diagonal lines represent a family of these predictions, denoted on the plot by the relative fraction $\Delta M_{\rm el}/M$ of the planet's mass that can be lost in XUV-driven escape. The upper green line $\Delta M/M = 0.2$ is the extension of the dashed magenta curve for XUV-driven energy-limited escape from tidally-truncated hot EGPs. The middle (solid) green line $\Delta M/M = 0.002$ approximates the upper bound ($f(H_2) = 1$) on diffusion-limited escape of H_2 for systems that are a few billion years old. The lower (dashed) green line $\Delta M/M = 0.0002$ approximates the upper bound on diffusion-limited escape of H_2 if rapid escape is restricted to young, XUV active stars.

It is notable that this ratio is very nearly independent of planetary parameters - i.e., this constraint is the same for all planets. For H_2 escaping through N_2, $b_{ij} \approx 1.5 \times 10^{19}\,(T/300)^{0.75}$, for which

$$\frac{\Delta M_{\rm dl}}{M} = 0.001 f({\rm H_2})\,(1000/T)^{0.25}\,\tau_{\rm Gyr} \tag{38}$$

with $\tau_{\rm Gyr}$ measured in Gyrs. This means that it is difficult for a planet to selectively lose more than about 0.5% of its mass as H_2 in 5 Gyr, even if H_2 is a major constituent ($f(H_2) \to 1$), as it often appears to be on exoplanets. In many XUV-limited escape scenarios the time available for energy-limited escape is less than a few hundred million years, which reduces the maximum differential H_2 loss to less than 0.05% of the planet's mass. Whether this is an important constraint depends on several factors. If H_2 is overwhelmingly abundant and the heavy gases are inefficient radiative coolants, they can be carried along, and $\phi_{i,{\rm dl}}$ becomes the difference between H_2 escape and heavy gas escape (Sekiya et al. 1981; Zahnle and Kasting 1986). If the heavy gases condense, they can be separated from H_2 by precipitation and the gas diffusion limit does not apply. But for warm planets with considerable reservoirs of volatiles other than H_2, the constraint may set the boundary between planets that evolve to a vaguely Earth-like state vs. those that never progress past a vaguely Neptune-like state. That XUV-driven escape should lead to such a bimodal distribution of planets has also been made on the basis of the limited XUV energy available (Owen and Wu 2013).

4.3. *Extrasolar Giant Planets*

The simple linear relation between $I_{\rm xuv}$ and x in Equation 33 does not apply for the close-in planets that are afflicted by tidal truncation. For these we need to include the Hill sphere terms, which break the $I_{\rm xuv} \propto x$ relation. For these

planets we start with a tidally truncated XUV-heated energy-limited escape flux,

$$\frac{\pi R^2 \eta L_{\rm xuv}}{4\pi a^2} = \frac{GM\dot{M}_{\rm el}}{R}\left(1 - \frac{3}{2}\frac{R}{r_h} + \frac{1}{2}\frac{R^3}{r_h^3}\right) \tag{39}$$

As above, we treat EGPs as all having the same radius R. With R held constant, M can be replaced by $v_{\rm esc}$; the star-planet distance a can be replaced by $I_{\rm xuv}$; and $M_\star$ is replaced $M_\odot$ by expressing $L_x/L_{x\odot} \propto (L_\star/L_\odot)^{0.4} \propto (M_\star/M_\odot)^{1.5}$, in which the stellar mass-luminosity relationship is conveniently written in the form $L_\star \propto M_\star^{3.75}$. With these relations, the $L_x/L_{x\odot}$ ratio cancels out of Eq 39. The resulting expression between $I_{\rm xuv}$ and $v_{\rm esc}$ should hold approximately for all main sequence stars and their giant planets,

$$\frac{a_3 I_{\rm xuv}}{v_{\rm esc}^4} = \frac{\Delta M_{\rm el}}{M}\left(1 - a_1\frac{I_{\rm xuv}^{1/2}}{v_{\rm esc}^{2/3}} + a_2\frac{I_{\rm xuv}^{3/2}}{P v_{\rm esc}^2}\right) \tag{40}$$

$$a_1 = \frac{3}{2}\frac{R}{P a_\oplus}\left(\frac{6GM_\odot}{R}\right)^{1/3}$$

$$a_2 = \frac{1}{2}\frac{R^3}{a_\oplus^3}\frac{6GM_\odot}{R}$$

$$a_3 = \frac{GR}{a_\oplus^2}\frac{\eta L_x t_x}{(\beta-1)}\left(\beta - (t_x/\tau_\star)^{\beta-1}\right).$$

Equation 40 is readily solved for $I_{\rm xuv}$ as a function of $v_{\rm esc}$. Results are plotted for $\Delta M_{\rm el}/M = 0.2$ with $\eta = 0.2$ as the dashed magenta lines on Figures 2 and 3. For the particular case with R held constant, $x \propto v_{\rm esc}^4$, so the curves are uniquely defined on both plots. As has been pointed out by others (e.g., Owen and Wu 2013), the quantitative predictions made by the simple XUV model are good enough to be intriguing.

5. IMPACT EROSION

Impact erosion of planetary atmospheres can be another path to ruin (Walker 1986; Melosh and Vickery 1989; Zahnle et al. 1992; Zahnle 1993, 1998a; Griffith and Zahnle 1995; Chen and Ahrens 1997; Brain and Jakosky 1998; Newman et al 1999; Genda and Abe 2003, 2005; Catling and Zahnle 2009; de Niem et al. 2012; Catling and Zahnle 2013; Schlichting et al. 2015). The basic idea is that a portion of a planetary atmosphere is blasted into space if an impact is big enough and energetic enough. Once in space the noncondensing volatiles are presumed dispersed by radiation pressure or the solar wind, whilst condensing materials are for the most part swept up again. In detail, how impact erosion actually works remains a work in progress. It may be that impact erosion is mostly caused by very large collisions that drive off much of the atmosphere in a single blow (Korycansky 1992; Chen and Ahrens 1997; Genda and Abe 2003, 2005), or it may be more like sandblasting, with tens of thousands of small impacts each doing a little (Walker 1986; Melosh and Vickery 1989; Zahnle et al. 1992), or it could be something in between, or a combination of all these effects. Moreover, impact erosion cannot be evaluated while not also evaluating the impact delivery of new volatiles.

In previous work, we suggested that impact erosion is likely to be dominated by numerous relatively small projectiles striking the planet's surface at velocities well in excess of the escape velocity, whilst impact delivery of new volatiles is likely to be dominated by a few slow-moving, very large volatile-rich bodies (Zahnle et al. 1992; Griffith and Zahnle 1995). Consequently, although the loss of atmosphere by impacts may be plausibly approximated by a continuous function, impact delivery of volatiles is likely to be profoundly stochastic. If this is how it works, impact erosion, when it gets the upper hand, will annihilate the atmosphere, because as the atmosphere thins the eroding projectiles become ever smaller and more numerous. This kind of impact erosion is a good candidate for creating a nearly airless world like Mars (Melosh and Vickery 1989; Zahnle 1993) and it readily accounts for the sharp distinction between the atmospherically-gifted Titan on one hand and the airless Callisto and Ganymede on the other (Zahnle et al. 1992; Griffith and Zahnle 1995; Zahnle 1998a). But where by chance a single late great impact delivers an atmosphere so massive that all subsequent impacts are insufficient to remove it, a considerable atmosphere can be left on a planet where one might not expect to find one (Griffith and Zahnle 1995). If impact erosion is the chisel that sculpts extra-solar systems, we would expect that by chance there will exist a few small, close-in planets enveloped in appreciable atmospheres. This may be germane to assessing Proxima b.

However it happens, it is plausible that the efficiency of impact erosion should scale as $v_{\rm imp} \propto v_{\rm esc}$, and therefore in Figure 4 we plot the planets on the grid $v_{\rm imp}$ *vs.* $v_{\rm esc}$. To prepare Figure 4 we use solar system impact velocities from (Zahnle et al. 2003) with appropriate updates for the KBOs. For the exoplanets we assume that the impacting bodies come from prograde orbits of modest inclination and eccentricity that generically resemble those of the asteroids and Jupiter-family comets that strike Earth and Venus. In the inner Solar system, encounter velocities $v_{\rm enc}$ are typically on the order of $0.5 - 1.0\times$ the orbital velocity, with the higher encounter velocity appropriate to matter falling from greater heights above the Sun (i.e., comets) (Bottke et al. 1995). The circular orbital velocity $v_{\rm orb}$ of an extrasolar planet is computed using the reported period and either the semimajor axis, such that $v_{\rm orb} = 2\pi a/P$, or the star's mass $M_\star$, such that $v_{\rm orb}^3 = 2\pi GM_\star/P$. For most planets a and $M_\star$ are both listed; for these we take the average. What is actually plotted on Figure 4 uses

$$v_{\rm imp}^2 = v_{\rm enc}^2 + v_{\rm esc}^2 \tag{41}$$

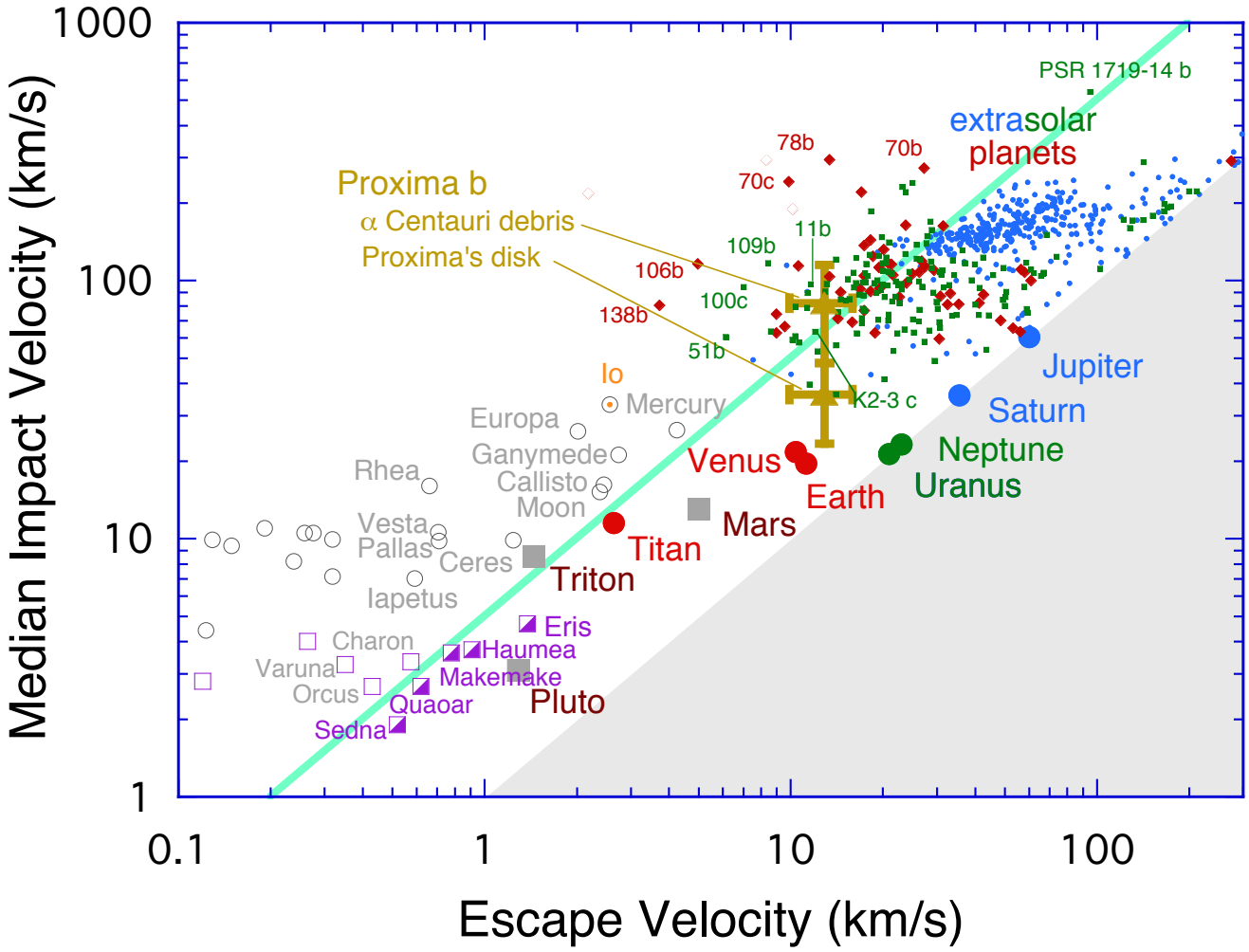

FIG. 4.— Here typical impact velocities, estimated from the orbital velocities $v_{\rm orb}$ of the planets, are plotted against $v_{\rm esc}$. The shaded area in the lower right is unphysical, because an impactor has to have a velocity that is minimally the escape velocity from energy conservation; we plot it this way because it looks nice. Solar System bodies with atmospheres, such as Earth, are plotted in solid colors. Bodies in the Solar System that are devoid of atmospheres are plotted with open gray symbols. Kuiper Belt Objects are purple. Transiting exoplanets are plotted in blue disks (Saturns and Jupiters), green boxes (Neptunes), and red diamonds (Venuses). Expansive error bars are omitted for clarity. The empirical impact erosion stability limit for solar system atmospheres is roughly $v_{\rm imp}/v_{\rm esc} = 5$. Proxima b is plotted twice (in gold). The upper point presumes impacts by bodies in orbit about α Centauri itself. The lower point presumes impacts by bodies revolving around Proxima in orbits roughly coplanar with Proxima b.

with $v_{\rm enc} = v_{\rm orb}$.

Although the data are very uncertain, Figure 4 shows clearly that impact erosion cannot be lightly dismissed. But we are not currently in a position to make quantitative predictions comparable to those we made for insolation-driven escape: we don't know the actual impact velocities anywhere other than in our own solar system, and even here we meet with considerable dispersion; nor do we know the volatile contents of the impacting bodies; nor do we have a robust theory of how impact erosion works; nor have we a robust theory to describe the retention and loss of the delivered volatiles. What we can say is that impact erosion has promise as a global explanation, and because its effects are roughly parallel to those of insolation-driven escape, the two processes might often work together. For what it is worth, the empirical dividing line for the ensemble, $v_{\rm imp} \approx 4-5\,v_{\rm esc}$, is at a higher $v_{\rm imp}$ than the $v_{\rm imp} \approx 2.5\,v_{\rm esc}$ that had been discussed for Mars (Melosh and Vickery 1989; Zahnle 1993). It may be germane that the ejecta from comet Shoemaker-Levy 9 were launched at 20-25% of the impact velocity (Zahnle 1996), which suggests to the optimist that the relation $v_{\rm imp} \approx 4-5\,v_{\rm esc}$ may hold generally for airbursts in deep atmospheres.

6. PROXIMA B: ON THE BEACH

In 2016, a planet somewhat more massive than Earth was discovered orbiting the Sun's nearest neighbor every 11.2 days (Anglada-Escudé et al. 2016). The planet lies within the conventional habitable zone, in that it intercepts a total amount of insolation comparable to what the Earth intercepted during its inhabited Archean Eon ca 3 Ga. This mix of qualities — the nearest exoplanet, vaguely Earth-massed, in the habitable zone — almost guarantees that Proxima

b will be explored by humans or their descendants at some point in the distant future. There has been a fair amount written about Proxima b that does not all need to be repeated here (Anglada-Escudé et al. 2016; Davenport et al. 2016; Ribas et al. 2016; Turbet et al. 2016; Barnes et al. 2017; Coleman et al. 2017; Goldblatt 2017; Meadows et al. 2017). Here we wish to document how we plotted Proxima b on Figures 1-4 and then, briefly, speculate about its habitability.

6.1. *Proxima b: escape velocity*

Proxima b's escape velocity is uncertain because we do not know its radius; we do not know whether it is a globe of air, water, earth, or metal. Radial velocity gives $M \sin i = 1.27 M_\oplus$. We presume the median nominal mass of $M_p = 1.27/\sin 60^\circ = 1.47 M_\oplus$. If rocky, using $M_p \propto R_r^{3.7}$ (Zeng et al. 2016), we estimate $v_{\rm esc} = 12.7$ km s^{-1}. To set a rough upper uncertainty we take a more face-on $\sin 30^\circ$ orbit, for which $v_{\rm esc} = 15.3$ km s^{-1}. To set a rough lower uncertainty, we presume that Proxima b is ice-rich with a bulk density half that of a rocky world of the same mass, for which $v_{\rm esc} = 10.2$ km s^{-1}.

6.2. *Proxima b: XUV heating*

For Proxima specifically, Ribas et al. (2016) estimate both the current and the cumulative relative XUV irradiations of Proxima b and Earth. It is a curious fact that Ribas et al. (2016) suggest that Proxima's XUV flux history has been roughly constant for most of the life of the star, which differs from the usual assumption that young stars are much stronger XUV sources than old stars, The reason for imposing this unusual history appears to be discomfort with the peculiarly active state of Proxima today. For the present, they estimate that $I_{\rm xuv}/I_\oplus \approx 60$. For the cumulative total, they estimate that $I_{\rm xuv}/I_\oplus \approx 16$. We plot both estimates on Figures 2 and 3, each with a factor 2 uncertainty. On Figure 2, Proxima b appears relatively vulnerable to XUV-driven escape. Only a big and dense Proxima b orbiting an XUV-quiet Proxima plots with the terrestrial planets of our solar system. Otherwise, Proxima b plots with the least of the extrasolar Neptunes and a few other smaller planets. But when the ensemble is replotted according to the expectations of energy-limited flux, Proxima b looks rather ordinary (Figure 3). Figure 3 also suggests that Proxima b at 0.05 AU has intercepted enough XUV energy to drive off about 1% of its mass; a waterworld Proxima b should be durable to XUV radiation if it could be made in the first place, but a more Earth-like hydrosphere could be vulnerable to being wholly lost.

6.3. *Proxima b: insolation*

After it formed, Proxima is presumed to have slowly faded to the main sequence like any small M dwarf. Figure 1 shows insolation levels from Ribas et al. (2016) at 3 times: when Proxima was just 10 Myr old, when Proxima was 100 Myr old, and today. With respect to total insolation, on Figure 1 Proxima b is much like Earth or Venus. As Ribas et al. (2016) and Barnes et al. (2017) and many others have pointed out, when Proxima was young, insolation exceeded the runaway greenhouse threshold at Proxima b's current 0.05 AU distance for the first $\sim$ 150 Myrs or so of their mutual existence (Barnes et al. 2017). This means that Proxima b, if it had water when young, would have held it initially in the form of steam. Other things equal, hydrogen more easily escapes from a steam atmosphere than from a liquid ocean or from ice sheets. If hydrogen escape is restricted to the runaway greenhouse epoch, estimates of the total XUV-driven energy-limited escape range from less than an Earth ocean of water Ribas et al. (2016) to 3-10 oceans (Barnes et al. 2017), a difference that can be attributed to assumptions about Proxima as a young star.

6.4. *Proxima b: oxygen*

It has been suggested that, if the source of escaping hydrogen is water, O_2 might build up in the atmosphere at the diffusion-limited rate, and if the hydrogen from several oceans of water escaped, it might be possible for hundreds of bars of O_2 to accumulate in the atmosphere left behind (Luger and Barnes 2015; Schaefer et al. 2016; Barnes et al. 2017). However, these models do not account for atmospheric photochemical reactions between oxygen and hydrogen that can reduce the H_2 mixing ratio so that $f(H_2) \ll 1$ and thus throttle hydrogen escape. For example, the hydrogen escape rate from Mars is currently very slow because the strong negative feedback between oxygen and hydrogen ensures that both are lost from the atmosphere in the 1:2 ratio of the parent molecule (Hunten and Donahue 1976). The same 1:2 ratio holds for oxygen and hydrogen escape from Venus today (Fedorov et al. 2011). Moreover, iron in a vigorously convecting mantle has the capacity to consume thousands of bars of O_2. For example, Hamano et al. (2013) dispose of the excess oxygen generated by hydrogen escape from Venus's accretional steam atmosphere by putting it into the mantle while still mostly molten under a steam atmosphere. In any event O_2 on Venus has yet to be detected (Fegley 2014). Schaefer et al. (2016) include aspects of the kinetics of the mantle sink. If the XUV is very large, hydrogen escape can in principle be vigorous enough to drag the oxygen liberated by water photolysis into space (Zahnle and Kasting 1986; Luger and Barnes 2015; Schaefer et al. 2016). For example, Zahnle and Kasting (1986, Fig. 8) showed that for conditions germane to a steam atmosphere on Venus, molecular diffusion ensures that oxygen escape must exceed the surface sink on oxygen, no matter how efficient the latter. Schaefer et al. (2016) reached a similar conclusion for GJ 1132b and other worlds. When hydrogen escape exceeds the diffusion limit, the diffusion limit becomes the rate that oxygen is left behind to oxidize the planet or accumulate in the atmosphere. However, in addition to not including atmospheric chemistry, neither model took into account that because the mixed wind is heavier, it must be hotter than pure hydrogen and thus has more power to cool itself radiatively. It is possible that radiative cooling by the enhanced abundance of heavy atoms embedded in the flow will provide effective thermostatic control over the rate of escape.

6.5. *Proxima b: impacts and impact erosion*

The history and nature of impacts experienced by Proxima b are almost wholly conjectural (Coleman et al. 2017). Still, impacts happen. It may be helpful to divide impactors into three general classes: (i) material co-orbital with Proxima b; (ii) material in orbits about Proxima (analogous to the Sun's asteroid and Kuiper belts) and (iii) material in orbits about α Centauri A or B or both (Kuiper belts and Oort clouds would be Solar System analogs). The first category is swept up very quickly and is better regarded as part of Proxima b's accretion and will be addressed separately below. In the second category we imagine bodies in prograde orbits roughly coplanar with Proxima b and perturbed from relatively distant orbits, with aphelia at say 1 AU, into highly elliptical Proxima b-crossing orbits. By analogy to impacts on Earth (Bottke et al. 1995), we estimate that typical encounter velocities would be of the order of $\langle v_{\rm enc}\rangle \approx 0.5 - 0.8\, v_{\rm orb}$, which corresponds to $v_{\rm imp} \approx 30 \pm 15$ km s^{-1}. The third category is analogous to the comets and asteroids that strike the Galilean satellites (in mildly hyperbolic orbits with respect to Juoiter), with almost all of the velocity of the stray body attributable to the gravitational well of the central body. We have previously modeled this scenario for the Galilean satellites, taking into account the distribution of impact probabilities associated with the distribution of encounter orbits (Zahnle et al. 1998b). Generalizing from Zahnle et al. (1998b), we estimate that close encounters of the third kind would fall in the range $v_{\rm enc} \approx 1.4 - 2.4\, v_{\rm orb}$; i.e., we estimate that $v_{\rm enc} \approx 90 \pm 25$ km s^{-1}. Cases (ii) and (iii) are plotted on Figure 4. It is apparent at a glance that Proxima b is more vulnerable to the negative consequences of impacts than are Earth and Venus, a not surprising observation that has been anticipated (cf, Raymond et al. 2007; Lissauer 2007). We conclude that almost all the collisions that matter to impact erosion and impact delivery must be from debris orbiting Proxima itself, at velocities that are marginally more erosive than what we see in the inner Solar System.

6.6. *Proxima b: accretional heating*

If averaged over 100 Myrs, the energy of accretion of a planet like Earth is comparable in magnitude to the insolation over that same period. This was very important for Earth and Venus because they likely accreted on a 30-100 Myr timespan, and the added energy of accretion pushed both planets above their runaway greenhouse limits (Matsui and Abe 1986; Abe and Matsui 1988; Zahnle et al. 1988; Hamano et al. 2013). For Earth, the steam atmospheres were episodic transients after big impacts, but Venus's steam atmosphere was probably irreversible, and hence led directly to the profound desiccation of Venus's atmosphere and mantle (Hamano et al. 2013).

By contrast to Earth and Venus, Proxima b could have accreted very quickly. Lissauer (2007) showed that in basic Safronov accretion theory, HZ (habitable zone) planets of small M dwarfs are expected to accrete in less than 10^5 years, orders of magnitude faster than Earth or Venus. Accretion in 10^5 years implies a surface temperature of 2000 K if airless and perhaps 4000 K if the planet had an atmosphere, which at temperatures like these it most certainly would have had (Lupu et al. 2014). In its potential for rapid accretion Proxima b is more like a Galilean satellite than a Solar System planet. The comparable accretion time for Europa is 200 years, which scarcely seems credible for a small world that retains a lot of water, to say nothing of icy Callisto accreting in just 3000 years yet never fully melting. Evidently Europa's and Callisto's accretions were governed by the supply of new matter from the Sun's accretion disk to Jupiter's accretion disk, rather than by the properties of Jupiter's accretion disk. The ruling time scale then becomes that of forming the solar system as a whole, which appears to have been on the order of 3 million years (and slow enough to preserve a cold Callisto). But Proxima b is much bigger than Europa or Callisto. Even if material were supplied to the Proxima system from an unknown source on a more leisurely 10 million year time scale, Proxima b's accretion would not only be too rapid for water to condense, it would be too rapid for a magma surface to freeze solid unless there were no atmosphere (Lupu et al. 2014).

6.7. *Proxima b: Stellar Wind*

Here we ask if atmospheric erosion by Proxima's stellar wind has been important. In the Solar System, the solar wind erodes through direct collisions (sputtering) and through its magnetic field (ion pickup). The latter in particular is important for Venus and Mars. Venus intercepts about 4000 grams of solar wind per second, estimated using $\dot{M}_\odot = 2 \times 10^{-14} M_\odot$ yr^{-1} (Wood et al. 2002). Average quiet sun observed rates of oxygen ion escape from Venus are much smaller, about 150 g s^{-1} (Fedorov et al. 2011). Modeled O^+ escape rates range from 150 to 800 g s^{-1} (Jarvinen et al. 2009). Solar wind driven escape at Mars is more efficient: Mars intercepts about 300 grams of solar wind each second, which is comparable to the observed O^+ escape rate of 160 g s^{-1} (Brain et al. 2015) and to modeled O^+ escape rates of 300 – 500 g s^{-1} (Lammer et al. 2003b). Apparently the solar wind impinging on Mars erodes roughly its own mass in martian atmosphere, although Venus suggests that escape processes are, among other things, sensitive to $v_{\rm esc}$.

Suppose that the observed martian regime approaches the asymptotic efficiency. This may be a reasonable bound on a process that in broad brush is a problem of turbulent mixing. If so, the planet's mass loss rate would be equal to the mass of stellar wind intercepted,

$$\dot{M} = \frac{\pi R^2}{4\pi a^2} \dot{M}_{\rm sw}, \tag{42}$$

where $\dot{M}_{\rm sw}$ is the star's mass loss rate. The stellar wind is assumed strong enough that the planet's cross section to the wind is comparable to its physical cross section. Proxima b therefore intercepts 1×10^{-6} of $\dot{M}_{\rm sw}$. We estimate that $\dot{M}_{\rm sw}$ for Proxima today is roughly $3 \times 10^{-15} M_\odot$ yr^{-1}, in which we have scaled the solar wind by XUV (Wood

et al. 2002). If we assume that $\dot{M}_{\rm sw} \propto t^{-1}$, we estimate that Proxima b has intercepted roughly 1×10^{23} g of stellar wind since it first became potentially habitable at 150 Myr of age. This corresponds to 1×10^{-5} of Proxima b's mass, or about 10 bars of atmosphere. Losses would be less than 1 bar if the extrapolation were based on Venus. These estimates are respectively 2 and 3 orders of magnitude smaller than what XUV can do in the first 150 Myr for an H_2-rich or H_2O-rich atmosphere (Barnes et al. 2017). On the hand, the stellar wind might pose the greatest existential threat to a CO_2 atmosphere at times after the first 150 Myrs.

6.8. *Proxima b: "Ashes, Ashes and Dust, and Thirst there is"*

Proxima b may have no good analog in the Solar System, then again it may. Venus seems the best candidate for an analog. Venus retains very little water (in the atmosphere, 5×10^{-6} of Earth, Fegley (2014)) and probably very little in its interior. Hamano et al. (2013) explains Venus as having been thoroughly desiccated by hydrogen escape from a steam atmosphere over a molten silicate surface that lasted for more than 100 Myrs. In this picture the mantle remained in equilibrium with the water vapor in the atmosphere, and thus the loss of all the water from the atmosphere meant also the loss of almost all the water from the mantle. Both early insolation and accretional energy are greater for Proxima b than for Venus, which makes Venus's story seem all too likely Proxima b's story as well.

Mercury and Io represent end members where the forces of escape (for Mercury, insolation and XUV; for Io, impact erosion and perhaps infrared radiation from Jupiter when young) are almost wholly victorious. Both retain sulfur. Notably, Mercury appears to retain about as much water as it can harbor in its shadowed craters, which is empirical evidence either that high speed impacts do not wholly preclude the accretion of small amounts of water, or that even a planet as blasted as Mercury can still degas a little water. Mars may be a guide to what Proxima b might look like if it were in equilibrium with a late bombardment (post-dating the runaway greenhouse phase) of volatile-rich bodies dislodged from cold distant orbits. Between Mercury and Mars there is a place for a habitable desert state for Proxima b (Abe et al. 2011; Turbet et al. 2016).

Europa and Ganymede are examples of planets born with too much water to lose. We argued with respect to Figure 3 that over 5 Gyr it is difficult for any planet, no matter how small or strongly irradiated, to selectively lose more than about 0.2% of its mass as hydrogen, so that an initial water inventory greater than say 2% by mass is likely not to be lost save by impact erosion. Both Europa and Ganymede appear to have been heated well enough during accretion that they are thoroughly differentiated, yet each retains a lot of water (Europa is $\sim 7\%$ water, Ganymede nearly 50%). How a water world Proxima b might accrete is a puzzle — perhaps a giant impact of a stray water rich planet with a local planet could do it — but given the current absence of a predictive model of planetary accretion, nothing should be ruled out (Lissauer 2007; Ribas et al. 2016; Barnes et al. 2017; Coleman et al. 2017).

Earth would be the best of all possible analogs, at least from the explorer's point of view, but the real Earth's hydrosphere is too thin to have survived Proxima's youthful luminosity and the onslaught of XUV radiation and flares that continues today (Davenport et al. 2016). Both Ribas et al. (2016) and Barnes et al. (2017) explicitly construct habitable states by starting with just enough water that the loss of the hydrogen from some 1-10 oceans of water leaves an ocean or so behind after the early steam atmosphere condensed. Lissauer (2007) pointed out that an Earth-like outcome in this scenario, or in any of several other scenarios he considered, requires "precisely the right amount of initial water or just the right dynamics." I.e., Earths are unlikely outcomes for Proxima b compared to a vastly greater phase space of less happy outcomes. When conceiving *Kepler,* Borucki et al. (1996) set out to determine the number of Earth-like planets in the cosmos by direct observation. With all apologies to theory, this remains the path forward.

7. DISCUSSION

In this paper we have discussed the empirical evidence for a cosmic shoreline uniting the worlds of the Solar System with the exoplanets whilst dividing the worlds between those with apparent atmospheres and those without. This is done through four figures, each of which compares the potency of a loss process to the planet's ability to hold an atmosphere, and each of which shows roughly the same pattern.

Figure 1 finds the known worlds sorting themselves according to a simple $I \propto v_{\rm esc}^4$ power law relating total insolation to escape velocity. Thermal escape driven by the total insolation is best regarded as a function of the sound speed $c_\circ^2 = k_B T/\bar{m}$, because it is as sensitive to the mean molecular weight $\bar{m}$ as it is to the temperature T. It is reasonable then to expect the shoreline to look like $c_\circ^2 \propto v_{\rm esc}^2$. We expect that $\bar{m}$ will be of order 20 for terrestrial planets, ~ 2.4 for the cooler giant planets, and of order 1 for the hottest planets in which H_2 is dissociated to atoms. If by Stefan-Boltzmann's law $I \propto T^4$, and if by chemistry we ask that $\bar{m} \propto T^{-1}$, we can recover the empirical $I \propto v_{\rm esc}^4$ relation. We also show that a relatively simple thermal evaporation model with tidal truncation provides a credible boundary to the highly irradiated extrasolar giant planets (EGPs). Total insolation provides more scope for explaining the enhanced erosion seen in the most massive and most strongly heated EGPs than does energy-limited XUV-driven escape, which by construction depends only on XUV irradiation and does not depend on T or $\bar{m}$. In particular, total insolation-driven escape can greatly exceed the XUV-driven energy limit.

Figures 2 and 3 address energy-limited XUV-driven escape. The relevant quantity — the cumulative historic XUV irradiation at each planet, which is dominated by the excesses of the young star — is not an observable. Both plots are constructed by creating a proxy quantity $I_{\rm xuv}$ that is scaled from the Sun; the plots are then to be regarded as comparing other systems to the Solar System. The plots can also be viewed as proxies for stellar wind-driven escape, as stellar winds stem from the same sources as the nonthermal X-rays and EUV radiations. Figure 2 looks much like Figure 1 because the Sun is the same in a relative way on both plots. The figures differ only in how the exoplanets

are plotted. Here we see a wider scatter of small planets that according to our hypothesis would have to be airless, and we see a tidier distribution of highly irradiated EGPs. We confirm that energy-limited XUV-driven escape also provides a credible quantitative boundary to the EGPs.

Figure 3 explores XUV-driven escape more generally in terms of a scaling parameter that encapsulates the $I \propto v_{\rm esc}^3 \sqrt{\rho}$ shorelines predicted by energy-limited escape. The figure provides context in which to discuss the limits to diffusion-limited flux. The division between planets that are born with too much hydrogen to lose corresponds to about 0.2% H_2 by mass or, equivalently, about 2% H_2O by mass. Owen and Wu (2013) previously reached a similar conclusion based on energy considerations. The diffusion bound is an upper bound because it does not taken into account that the energy-limited flux is often the smaller, as it would have been for Earth itself (whose upper bound on selective H_2 escape is less than 0.05% by mass), and it does not account for escape slowing down as the atmospheric mixing ratio of H_2 shrinks.

Figure 4 addresses the competition between impact delivery of volatiles and impact erosion of atmospheres as an alternative to irradiation-driven escape. Here we expect the shoreline to take a simple form in which the typical impact velocity $v_{\rm imp}$ is proportional to the escape velocity $v_{\rm esc}$. Unfortunately impacts are poorly described by a single size of a single composition striking at a single impact velocity. Rather, stray bodies have many sources, so that even in our Solar System there is considerable uncertainty in the cumulative effects produced by the different sizes, compositions, velocities, and impact geometries of the impacting bodies. What we have done for the extrasolar planets is equate $v_{\rm imp}$ to the circular orbital velocities $v_{\rm orb}$ of the planets, because for impact velocities to be high enough to matter, the velocities of the colliding bodies will be determined by the gravity of the central star. The empirical impact shoreline then follows the quantitative relation $v_{\rm imp} \approx 4{-}5\, v_{\rm esc}$. The proportionality constant agrees with what one would extrapolate from the observed consequences of the impact of Comet Shoemaker-Levy 9 with Jupiter. In the Shoemaker-Levy 9 impacts the bulk of the ejecta, much of which was shocked jovian air as fingerprinted by the chemical composition of the ejecta, were launched at 12-15 km s^{-1}; i.e., at 20-25% of the impact velocity (Zahnle 1996). This gives one some reason to think that the factor of $4-5$ might be generally relevant to modest impacts in deep giant planet atmospheres. It may be reasonable to expect a lower threshold for impact erosion from planets with well-defined surfaces (Melosh and Vickery 1989), yet the different fates of Titan and Callisto can be nicely accounted for by the same factor of $4-5$.

Finally, it has probably not escaped the reader's attention that throughout this essay we have conflated giant planets (with giant atmospheres) with the Solar System's terrestrial planets (with thin atmospheres). This is partly necessity — we do not yet have the tools to identify thin atmospheres amongst the exoplanets — but there is also philosophy. First, there is interest: the cosmic shoreline is where we live and is where we think life is likeliest to flourish. Second, we do not know if the shoreline is broad or narrow (i.e., whether the transition from a thin atmosphere to one too thick and deep to be habitable to an ecology like our own is gentle or abrupt), nor in what ways our Solar System is representative or unrepresentative of extrasolar systems. In this essay we have chosen to arrange things to unify the many worlds of the cosmos.

8. ACKNOWLEDGEMENTS

Your name could go here. Impress your peers. The best comments and criticisms will be rewarded with acknowledgements.

All credit should go to the discoverers of the exoplanets for the new worlds that they have given us. On a smaller scale, the authors thank in particular CZ Goldblatt, MS Marley, and VS Meadows for pestering them for 9 years to write this up. This work was funded by NASA Planetary Atmospheres grant NNX14AJ45G and NASA Astrobiology Institutes Virtual Planetary Laboratory under Cooperative Agreement Number NNA13AA93A.

REFERENCES

Abe Y., Matsui T. (1988). Evolution of an impact-generated H2O–CO2 atmosphere and formation of a hot proto-ocean on Earth. *J. Atmos. Sci. 45,* 3081–3101.

Abe Y, Abe-Ouchi A, Sleep NH, Zahnle KJ (2011). Habitable Zone Limits for Dry Planets. *Astrobiology 11,* 443-460.

Anglada-Escudé G. and 32 others (2016). A terrestrial planet candidate in a temperate orbit around Proxima Centauri,. *Nature 536,* 437-440.

Barnes R.K. and 14 others (2017) The Habitability of Proxima Centauri b: II: Evolutionary Scenarios. *Astrobiology* arXiv:1608.06919v1

Bolmont E, Selsis F, Owen, JE, I. Ribas I, Raymond SN, Leconte J, Gillon M (2017). Water loss from terrestrial planets orbiting ultracool dwarfs: implications for the planets of TRAPPIST-1. *Mon. Not, Roy. Astron. Soc. 464,* 3728-3741.

Borucki WJ, Dunham EW, Koch DG, Cochran WD, Rose JD, Cullers DK, Granados A, Jenkins JM (1996). FRESIP: A mission to determine the character and frequency of extra-solar planets around solar-like stars. *Astrophys. Space Scii. 241,* 111-134.

Borucki WJ and others (2010). Kepler planet-detection mission: introduction and first results. *Science 327,* 977-980.

Bottke W.F., Nolan M.C., Greenberg R., Kolvoord R.A. (1995). Collisional lifetimes and impact statistics of near-Earth asteroids. In: *Hazards Due to Comets and Asteroids* (ed Gehrels T). Univ. of Arizona Press, Tucson, pp. 337-357.

Braga-Ribas F, Sicardy B, Ortiz JL, Lellouch E, Tancredi G, and 51 others (2013). The Size, Shape, Albedo, Density, and Atmospheric Limit of Transneptunian Object (50000) Quaoar from Multi-chord Stellar Occultations. *Astrophys. J. 773,* 26.

Brain D., Jakosky B. (1998). Atmospheric loss since the onset of the martian geologic record: Combined role of impact erosion and sputtering. *J. Geophys. Res. 103,* 22689–22694.

Brain D. and 19 others (2015). The spatial distribution of planetary ion fluxes near Mars observed by MAVEN. *J. Geophys. Res.* 10.1002/2015GL065293. (7 pp).

Brown ME (2013). On the size, shape, and density of dwarf planet Makemake. *Astrophys. J. Lett. 767,* L7(5pp).

Brown ME, Schaller EL (2007). The Mass of Dwarf Planet Eris. *Science 316,* 1585-1588.

Catling, D.C., Kasting, J.F. (2017). *Atmospheric Evolution on Inhabited and Lifeless Worlds.* New York: Cambridge University Press.

Catling DC, Zahnle, KJ (2009). The Planetary Air Leak. *The Scientific American 300,* 36-43.

Catling DC, Zahnle, KJ (2013). An impact erosion stability limit controlling the existence of atmospheres on exoplanets and solar system bodies. *Lun. Plan. Sci. Conf. 44,* 2665.

Chen GQ, Ahrens TJ. (1997). Erosion of terrestrial planet atmosphere by surface motion after a large impact. *Phys. Earth Planet. Int. 100,* 21-26.

Claire M.W., Sheets J., Cohen M., Ribas I., Meadows V.S., Catling D.C. (2012). The Evolution of Solar Flux from 0.1 nm to 160 μm: Quantitative Estimates for Planetary Studies. *Astrophys. J. 757,* 95 (12 pp).

Coleman G.A.L., Nelson R.P., Paardekooper S.J., S. Dreizler S., B. Giesers B., Anglada-Escudé G. (2017). Exploring plausible formation scenarios for the planet candidate orbiting Proxima Centauri. *Mon. Not, Roy. Astron. Soc.* arXiv:1608.06908v1.

Davenport J.R.A., Kipping D.M, Sasselov D., Matthews J.M., Cameron C. (2016). *MOST* observations of our nearest neighbor: flares on Proxima Centauri. *Astrophys. J. Lett. 829,* id L31 (5pp).

de Niem D., Kürht E., Morbidelli A., Motschmann U. (2012). Atmospheric erosion and replenishment induced by impacts upon the Earth and Mars during a heavy bombardment. *Icarus 221,* 495-507.

Erkaev NV, Kulikov Yu.N., Lammer H, Selsis F, Langmayr D, Jaritz GF, Biernat HK (2007). Roche lobe effects on the atmospheric loss from "Hot Jupiters". *Astron. Astrophys. 472,* 329-334.

Erkaev N.V., Lammer H., Odert P., Kulikov Yu., Kislayakova K.G., Khodachenko M.L., Güdel M., Hanslmaier A., Biernat H. (2013). XUV exposed non-hydrostatic hydrogen-rich upper atmospheres of terrestrial planets. Part I: Atmospheric expansion and thermal escape. *Astrobiology 13,* 1011-1029.

Erkaev N.V., Lammer H., Odert P., Kulikov Yu., Kislayakova K.G. (2015). Extreme hydrodynamic atmospheric loss near the critical thermal escape regime. *Mon. Not. Roy. Soc. 448,* 1916-1921.

Erkaev N.V., Lammer H., Odert P., Kislayakova K.G., Johntone C.P., Güdel M., Khodachenko, M.L. (2016). Thermal mass loss of protoplanetary cores with hydrogen-dominated atmospheres: The influences of ionization and orbital distance. *Mon. Not. Roy. Soc. 460,* 1300-1309.

Fedorov A, Barabash S, Sauvaud J-A, Futaana Y, Zhang TL, Lundin R, Ferrier C (2011), Measurements of the ion escape rates from Venus for solar minimum. *J. Geophys. Res. 116,* 07220 (7 pp).

Fegley B (2014). Venus. In *Planets, Asteroids, and the Solar System. Treatise on Geochemistry, 2nd Edition.* A.M. Davis (Ed.), Elsevier, pp. 127-148.

Fornasier S, and 19 others (2013). TNOs are Cool: A survey of the trans-Neptunian region. VIII. Combined Herschel PACS and SPIRE observations of 9 bright targets at 70500 μm. *Astron. Astrophys. 555,* A92.

Fortney JJ, Lodders K, Marley MS, and Freedman RS (2008). A Unified Theory for the Atmospheres of the Hot and Very Hot Jupiters: Two Classes of Irradiated Atmospheres. *Astrophy. J. 678,* 1419-1435.

Fray N., Schmidt B. (2009). Sublimation of ices of astrophysical interest: A bibliographic review. *Planet. Space Sci. 57,* 2053-2080.

Garcia-Munoz A. (2007). Physical and chemical aeronomy of HD 209458b. *Planet. Space Sci. 55,* 1426–1455.

Genda H., Abe Y. (2003). Survival of a proto-atmosphere through the stage of giant impacts: the mechanical aspects. *Icarus 164,* 149-162.

Genda H., Abe Y. (2005). Enhanced atmospheric loss on protoplanets at the giant impact phase in the presence of oceans. *Nature 433,* 842-845.

Gladstone G.R. and 32 others. The atmosphere of Pluto as observed by New Horizons. *Science 351,* 1280.

Griffith C.A., Zahnle K.J. (1995) Influx of volatiles to planetary moons: The atmospheres of 1000 possible Titans. *J. Geophys. Res. 100,* 16907-16922.

Goldblatt C. (2015). Habitability of waterworlds: Runaway greenhouses, atmospheric expansion, and multiple climate states of pure water atmospheres. *Astrobiology 15(5),* 362–370.

Goldblatt C. (2017). Tutorial models of the climate and habitability of Proxima Centauri b: a thin atmosphere is sufficient to distribute heat given low stellar flux. Submitted to *Astrophys. J. Lett.* arXiv:1608.07263

Goldblatt C., Robinson T.D., Zahnle K.J., D. Crisp D. (2013). Low simulated radiation limit runaway greenhouse climates. *Nature Geosci., 6,* 661–667.

Hamano, K., Abe, Y., Genda, H. (2013). Emergence of two types of terrestrial planet on solidification of magma ocean. *Nature 497,* 607-610.

Hayashi C., Nakazawa K., Mizuno H. (1979). Earth's melting due to the blanketing effect of the primordial dense atmosphere. *Earth Planet. Sci. Lett. 43,* 22–28.

Hubbard W. (1973). Interior of Jupiter and Saturn. *Ann. Rev. Earth Planet. Sci. 1,* 85-106.

Hunten DM (1990). Kuiper Prize Lecture: Escape of Atmospheres Ancient and Modern. *Icarus 85,* 1-20.

Hunten DM, Donahue TM (1976). Hydrogen loss from the terrestrial planets. *Ann. Rev. Earth Planet. Sci. 4,* 265-292.

Hunten DM, Pepin RO, Walker JCG (1987). Mass Fractionation in Hydrodynamic Escape. *Icarus 69,* 532-549.

Ikoma M., Genda H. (2006). Constraints on the mass of a habitable planet with water of nebular origin. *Astrophys. J. 648,* 696–708.

Jarvinen J, Kallio E, Janhunen P, Barabash S, Zhang TL, Pohjola V, Sillanpää I (2009). Oxygen ion escape from Venus in a global hybrid simulation: role of the ionospheric O^+ ions. *Ann. Geophys. 27,* 4333-4348.

Koskinen T.T., Aylward A.D., Miller S. (2009). A stability limit to the atmospheres of extrasolar giant planets. *Nature 450,* 845–848.

Koskinen TT, Yelle RV, Snowden DS, Lavvas P, Sandel BR, Capalbo FJ, Benilan Y, West RA (2011). The mesosphere and thermosphere of Titan revealed by Cassini/UVIS stellar occultations. *Icarus 216,* 507-534.

Koskinen TT, Harris MJ, Yelle RV, Lavvas P (2013). The escape of heavy atoms from the ionosphere of HD209458b. I. A photochemical-dynamical model of the thermosphere. *Icarus 226,* 1678-1694.

Koskinen T.T., Lavvas P., Harris M.J., Yelle R.V. (2014). Thermal escape from extrasolar giant planets. *Phil. Trans. Roy. Soc. A 372,* id 20130089 (12 pp).

Lammer H., Selcis F., Ribas I., Guinan E.F., Bauer S.J., Weiss W.W. (2003). Atmospheric loss of exoplanets resulting from stellar X-ray and Extreme Ultraviolet heating. *Astrophys. J. 598,* L21-L24.

Lammer H, Lichtenegger HIM, Kolb C, Ribas I, Guinan EF, Abart R, Bauer SJ (2003). Loss of water from Mars: Implications for the oxidation of the soil. *Icarus 165,* 9-25.

Lammer H. and 17 others (2009). Determining the mass-loss limit for close-in exoplanets: what can we learn from transit observations? *Astron. Astrophys. 506,* 399-410.

Lammer H., Erkaev N.V., Odert P., Kislyakova K.G., Leitzinger M., Khodachenko M.L. (2013). Probing the blow-off criteria of hydrogen-rich 'super-Earths'. *Mon. Not. Roy. Astron. Soc. 430,* 1247–1256.

Lammer H., Erkaev N.V., Dorfi E.A., Odert P., Güdel M., Kulikov Yu.N., Kislyakova K.G., Leitzinger, M. (2014). Origin and loss of nebula-captured hydrogen envelopes from 'sub'- to 'super-Earths' in the habitable zone of Sun-like stars. *Mon. Not. Roy. Astron. Soc. 439,* 3225–3238.

Lecavelier des Etangs A., Vidal-Madjar A., McConnell J.C., Hébrard G. (2004). Atmospheric escape from hot Jupiters. *Astron. Astrophys. 418,* L1-L4.

Leconte J.F., Forget F., Charnay B., Wordsworth R.D., Pottier A. (2013a). Increased insolation threshold for runaway greenhouse processes on Earth-like planets. *Nature 504,* 268–271.

Leconte J.F., Forget F., Charnay B., Wordsworth R.D., Selcis F., Millour E., Spiga, A. (2013b). 3D climate modeling of close-in land planets: Circulation patterns, climate moist bistability, and habitability *Astron. Astrophys. 554,* article 69 (17 pp).

Lehmer O., Catling D.C., Zahnle K.J. (2017). The longevity of water ice on Ganymedes and Europas around migrated giant planets. Submitted to *Astrophys. J.*

Lellouch E, and 16 others (2013). TNOs are Cool: A survey of the trans-Neptunian region. IX. Thermal properties of Kuiper belt objects and Centaurs from combined Herschel and Spitzer observations. *Astron. Astrophys. 557,* A60.

Lissauer, J.J. (2007). Planets formed in habitable zones of M dwarf stars probably are deficient in volatiles. *Astrophys. J. Lett. 660(2),* L149.

Lissauer J.J., Dawson R.I., Tremaine S. (2014). Advances in exoplanet science from Kepler. *Nature 513,* 336–344.

Lopez E., Fortney J.J. (2014). Understanding the mass-radius relation for sub-Neptunes: radius as a proxy for composition. *Astrophys. J. 792,* article id 1 (17 pp).

Luger R, Barnes R (2015). Extreme water loss and abiotic O2 buildup on planets throughout the habitable zones of M dwarfs. *Astrobiology 15,* 119-143.

Lupu RE, Zahnle KJ, Marley MS, Schaefer L, Fegley B, Morley C, Cahoy K, Freedman R, Fortney JJ (2014). The atmospheres of earthlike planets after giant impact events. *Astrophys. J. 784,* article id 27 (19 pp).

Korycansky D.G. (1992). An off-center point explosion in a radially stratified medium – Kompaneets approximation. *Astrophys. J. 398,* 184-189.

Korycansky D.G., Zahnle K.J. (2011). Titan impacts and escape. *Icarus 211,* 707-721.

Marten A, Matthews HE, Owen T, Moreno R, Hidayat T, Biraud Y (2005). Improved constraints on Neptune's atmosphere from submillimetre-wavelength observations. *Astron. Astrophys. 429,* 1097-1105.

Matsui T., Abe Y. (1986). Evolution of an impact-induced atmosphere and magma ocean on the accreting Earth. *Nature 319,* 303–305.

Meadows V.S., and 13 others (2017). The Habitability of Proxima Centauri b: II: Environmental States and Observational Discriminants. Submitted to *Astrobiology* arXiv:1608.08620.

Melosh HJ, Vickery AM (1989). Impact erosion of the primordial atmosphere of Mars. *Nature 338,* 487-489.

Murray-Clay R., Chiang E., Murray N. (2009). Atmospheric escape from hot Jupiters. *Astrophys. J. 693,* 23-42.

Nakajima S., Hayashi Y-Y., Abe Y. (1992). A study on the runaway greenhouse effect with a one-dimensional radiative-convective equilibrium model. *J. Atmos. Sci. 49,* 2256–2266.

Newman W.I., Symbalisty E.M.D., Ahrens T.J., Jones E.M. (1999). Impact erosion of planetary atmospheres: some surprising results. *Icarus 138,* 224-240.

Olkin C.B. and 19 others (1997). The thermal strucure of Triton's atmosphere: Results from the 1993 and 1995 occutations. *Icarus 129,* 178-201.

Owen J.E., Wu Y. (2013). *Kepler* planets: A tale of evaporation. *Astrophys. J. 775,* article 105 (12 pp).

Owen J.E., Alvarez M.A. (2016). UV-driven evaporation of close-in planets: Energy-limited, recombination-limited, and photon-limited flows. *Astrophys. J. 816,* article 34 (11 pp).

Pál A, and 16 others (2012). TNOs are Cool: A survey of the trans-Neptunian region. VII. Size and surface characteristics of (90377) Sedna and 2010 EK139. *Astron. Astrophys. 5541,* L6.

Perez-Becker D., Chiang E. (2013). Catastrophic evaporation of rocky planets. *Mon. Not, Roy. Astron. Soc. 433,* 2294-2309.

Rabinowitz DL, Barkume K, Brown ME, Roe H, Schwartz M, Tourtellotte S,Trujillo C (2006). Photometric Observations Constraining the Size, Shape, and Albedo of 2003 EL61, a Rapidly Rotating, Pluto-Sized Object in the Kuiper Belt. *AstrophysJ. 639(2),* 1238–1251.

Raymond S.N., Scalo J., Meadows V.S. (2007). A Decreased Probability of Habitable Planet Formation around Low-Mass Stars,. *Astrophys. J. 669,* 606–614, doi:10.1086/521587.

Ribas I., Guinan E.F., Güdel M., Audard M. (2005). Evolution of the solar activity over time and effects on planetary atmospheres. i. High-energy irradiances (11700Å). *Astrophys. J. 622,* 680-694.

Ribas I. and 11 others (2016). The habitability of Proxima Centauri b. *Astron. Astrophys. 596,* id A111 (18 pp.)

Robinson TD, Catling DC (2012). An analytic radiative-convective model for planetary atmospheres. *Astrophys. J. 757:* 104 (13pp).

Robinson TD, Catling DC (2014). Common 0.1 bar tropopause in thick atmospheres set by pressure-dependent infrared transparency. *Nature Geoscience 7,* 12-15.

Safronov, V. S. 1972. *Evolution of the Protoplanetary Cloud and Formation of the Earth and the Planets*, NASA Tech. Transl. F-677.

Schaefer L, Wordsworth R, Berta-Thompson Z, Sasselov D (2016). Predictions of the atmospheric composition of GJ1132b. *Astrophys. J. 829,* 63 (14pp).

Schaller EL, Brown ME (2007). Volatile loss and retention on Kuiper belt objects. *Astrophys. J. 659,* L61-L64.

Schlichting HE, Sari R, Yalinewich A (2015). Atmospheric mass loss during planet formation: The importance of planetesimal impacts. *Icarus 247,* 81-94.

Schneider J., Dedieu C., Le Sidaner P., Savalle R., Zolotukhin I. Defining and Cataloguing Exoplanets: the exoplanet.eu Database. *Astron. Astrophys. 532,* A79, 11pp.

Sekiya M., Nakazawa K., Hayashi C. (1980). Dissipation of the primordial terrestrial atmosphere due to irradiation of solar EUV. *Prog. Theor. Phys. 64,* 1968-1985.

Sekiya M., Nakazawa K., Hayashi C. (1980). Dissipation of the rare gases contained in Earth's primordial atmosphere. *Earth Planet. Sci. Lett. 50* 197-201.

Sekiya M., Nakazawa K., Hayashi C. (1981). Dissipation of the Primordial Terrestrial Atmosphere Due to Irradiation of the Solar Far-UV during T-Tauri Stage. *Prog. Theor. Phys. 68,* 1301-1316.

Sicardy B, Ortiz JL, Assafin M, Jehin E, Maury A, Lellouch E, Gil-Hutton R, Braga-Ribas F, Colas F, Widemann X (2011). Size, density, albedo and atmosphere limit of dwarf planet Eris from a stellar occultation. *European Planetary Science Congress Abstracts 6,* 137.

Stern SA and 42 others (2015). The Pluto system: Initial results from its exploration by New Horizons. *Science, 350,* aad1815, doi:1810.1126/science.aad1815.

Tian F., Toon O.B., Pavlov A.A., De Sterck H. (2005). Transonic hydrodynamic escape of hydrogen from extrasolar planetary atmospheres, *Astrophys. J. 621,* 1049–1060.

Tian, F. (2009). Thermal escape from super earth atmospheres in the habitable zones of M stars, *Astrophys. J. 703,* 905–909.

Tian F. (2015). Atmospheric Escape from Solar System Terrestrial Planets and Exoplanets. *Ann. Rev. Earth Planet. Sci. 43,* 459–476.

Turbet M., Leconte J., Selsis F., Bolmont E., Forget F., Ribas I., Raymond S., Anglada-Escudé, G. (2016). The Habitability of Proxima Centauri b II. Possible climates and observability. *Astron. Astrophys. 596,* id A112 (29 pp.)

Urey H.C. (1952). On the early chemical history of the earth and the origin of life. *Proc. Nat. Acad. Sci. 38,* 351–363.

Vidal-Madjar A., Lecavelier des Etangs A, Désert J-M, Ballester GE, Ferlet R, Hébrard G, Mayor M (2003). An extended upper atmosphere around the extrasolar planet HD 209458b. *Nature 422,* 143-146.

Vidal-Madjar A., Désert JM, Lecavelier des Etangs A, Hébrard G, Ballester GE, Ehrenreich D., Ferlet R., McConnell JC, Mayor M, Parkinson CD (2004). Detection of oxygen and carbon in the hydrodynamically escaping atmosphere of the extrasolar planet HD 209458b. *Astrophys. J. 604,* L69-L72.

Walker JCG (1986). Impact erosion of planetary atmospheres. *Icarus 68,* 87-98.

Watson A., Donahue T.M., Walker J.C.G. (1981). The dynamics of a rapidly escaping atmosphere: applications to the evolution of Earth and Venus, *Icarus 48,* 150-166.

Wesley CF, Batygin K, Brown ME, Bouchez A (2013). The mass, orbit, and tidal evolution of the Quaoar–Weywot system. *Icarus 222,* 357-363.

Wolf E.T., Toon O.B. (2015). The evolution of habitable climates under the brightening Sun. *J. Geophys. Res. Atmos. 120,* 5775–5794, doi:10.1002/2015JD023302.

Wood BE, Müller H-R, Gary P. Zank GP, Linsky JL (2002). Measured Mass-Loss Rates of Solar-Like Stars as a Function of Age and Activity. *Astrophys. J. 574,* 412-425.

Yang J., Cowan N.B., Abbot D.S. (2013). Stabilizing cloud feedback dramatically expands the habitable zone of tidally locked planets. *Astrophys. J. 771,* L45.

Yelle, R.V. (2004). Aeronomy of extra-solar giant planets at small orbital distances, *Icarus 170,* 167-179.

Zahnle KJ, Kasting JF (1986). Mass Fractionation during Transonic Escape and Implications for Loss of Water from Mars and Venus. *Icarus 68,* 462-480.

Zahnle K, Kasting JF, Pollack JB (1988). Evolution of a Steam Atmosphere during Earth's Accretion. *Icarus 74,* 62-97.

Zahnle K, Pollack JB, Grinspoon D, L. Dones L (1992). Impact generated atmospheres over Titan, Ganymede, and Callisto. *Icarus 95,* 1-23.

Zahnle KJ (1993). Xenological constraints on the impact erosion of the early Martian atmosphere. *J. Geophys. Res. 98,* 10899-10913.

Zahnle KJ (1996). Dynamics and chemistry of SL9 plumes. In: Noll K., Weaver H.A., Feldman P.D. (Eds.). *The Impact of SL9 with Jupiter, IAU Conference Proceedings,* Cambridge Univ. Press, Cambridge UK, pp. 183-212.

Zahnle K. (1998). Origins of Atmospheres. In *Origins.* C.E. Woodward, J.M. Shull, H. Thronson, eds. *Astron. Soc. Pacific Vol. 148,* 364-391.

Zahnle K, Dones L, Levison H (1998). Cratering Rates on the Galilean Satellites. *Icarus 136,* 202-222.

Zahnle K, Schenk P, Sobieszczyk S, Dones L, Levison H (2003). Cratering rates in the outer solar system. *Icarus 163,* 263-289.

Zahnle KJ, Catling DC (2013). The cosmic shoreline. *Lun. Plan. Sci. Conf. 44,* 2787.

Zeng L, Sasselov D, Jakobsen S. (2016). Mass-radius relation for rocky planets based on PREM. *Astrophys. J. 819,* 127 (5pp).